Emanuele Guercini

Targeted nanoparticles for drug delivery and molecular imaging

Trondheim, June 2016

Supervisor: Sjoerd Hak

Norwegian University of Science and Technology
Faculty of Medicine

NTNU
Det medisinske fakultet

Abstract

This study involved experiments on signal colocalization between $\alpha_v\beta_3$ integrin and RGD conjugated nanoemulsions as well as studies on nanoemulsion distribution and differences between the internalization patterns of RGD-NE and RAD-NE over time. This study was carried out on HUVEC cells and they were experimented upon from the fourth until the seventh passage. The study involved the research of a suitable optimization protocol, that is, a replicable optimal method for cell seeding, experimentation and fixation that yields the best results in terms of cell plating efficiency and cell density after exposure to experimental conditions.

Cell plating efficiency ad well as density and morphology has been found to be optimal when cells were seeded in a concentration of 20.000 cells per µ-well in 300 µl of defined medium. Cells density and morphology was found to be satisfactory when cells were fixed for 5 minutes at room temperature with 300 µl of 3% paraformaldehyde solution in PBS.

Prior to the colocalization study, it was hypothesized that we would find strong evidences between αvβ3 integrin and RGD-NE, alas, this was not the case. More precisely in the period of nanoemulsion incubation, almost no evidence of signal colocalization was found. It was concluded from the study that either the experimental method was faulty or that signal colocalization did indeed happen but it was not present in the time points analysed by this experiment.

The last study on the internalization behaviour of nanoemulsion as well as its distribution over time, confirmed previous hypothesis on internalization patterns and internal nanoemulsion distribution

Preface

This project was carried out at the Norwegian University of Science and Technology, at the Department of Physics during the fall 2015 and spring 2016. I would like to give my special thanks to my supervisors Sjoerd Hak whose passion and guidance led me through a year full of exciting challenges. I would also like to thank Kristin G. Sæterbø for her kindness and her insight on HUVEC cell culture and Astrid Bjørkøy for training and assistance with confocal laser scanning microscopy as well as her insight on colocalization.

Table of Content

1 Introduction 1

2 Theory 3

HUVEC 4

$\alpha_v\beta_3$ integrin 4

Nanoemulsion 5

Exploiting the niche 5

Confocal Laser Scanning Microscope 6

Structure of the Confoca Laser Scanning Microscope 6

3 Materials 9

Nanoemulsions 9

Stains 10

Fixation 10

4 Methods 11

Cell culture 11

Confocal Laser Scanning Microscope settings 13

Point Spread Functions 13

Optimization of the experimental conditions 14

Optimization of seeding density 14

Optimization of Fixation 14

Optimization of Integrin staining 15

Optimization of CellMask™ stain 15

Studies on colocalization 16

Studies on internalization patterns, 3D 16

Optimization of seeding density 17

Optimization of Fixation 20

Optimization of Integrin staining 21

Optimization of CellMask™ stain 22
Optimized experimental conditions. 26
Studies on colocalization 28
Studies on nanoemulsion internalization patterns, 3D rendering analyses 31
Studies on nanoemulsion internalization patterns, ROI analyses 38
6 Discussion 43
Studies on cell seeding density 43
Studies on Fixation 44
Studies on colocalization 45
Studies on nanoemulsion internalization patterns 46
7 Conclusion 49
1. 8 References 51

1 Introduction

According to the World Health Organization cancer is among the leading causes of mortality, accounting for 8.2 million of deaths in 2012 and 14 million of new cases[1]. Novel drugs and therapeutic strategies are being developed every day and the amount of approved drugs is at the moment more than two hundred [2]. Still it's not enough for the amount of new cases is only expected to rise by 70% in the next two decades [3].

Nanoparticles provide a new and exciting approach to try to prevent this disease [4-6]. By understanding mechanisms underlying tumour angiogenesis [7-9] and by targeting [10, 11] or exploding tumour leaky vasculature (EPR Effect) [12] it is possible to develop more efficient drugs or deliver contrast agents for cancer imaging.

Human umbilical vein endothelial cells (HUVEC) have been a model for in vitro studies of $\alpha_v\beta_3$ integrin expression for multiple years [13] as well as having been used extensively for studying the pathophysiological mechanisms of different diseases [14].

Moreover, $\alpha_v\beta_3$ integrin was identified as a marker of angiogenic vascular tissue [15], and high expression of this receptor on cancer vasculature has led to the interest in $\alpha_v\beta_3$ integrin for research of a suitable cancer-targeted drug delivery [7-9]. Targeting $\alpha_v\beta_3$ integrin with RGD conjugated peptides has been the focus of recent years in drug developments [7-9, 16-23].

Overall, the study carried out in this thesis has three aims:

First, to find a good optimization protocol, which yields the best results in terms of cell plating efficiency and cell density after the fixation, antibody tagging and membrane staining experiments on HUVEC incubated with nanoemulsion. The second aim was to find evidence of signal colocalization between $\alpha_v\beta_3$ integrin and RGD conjugated nanoemulsions. Eventually, the third aim was to investigate nanoemulsion distribution patterns inside HUVEC over time as well as the difference in distribution between cells exposed to RGD conjugated nanoemulsions and RAD conjugated nanoemulsions.

2 Theory

In this chapter, the background information required to understand the methodology and the results for the study are presented.

Cancer and angiogenesis

Cancer is a genetic disease in the sense that it is caused by a mutation in regulatory genes in the DNA [1]. This mutation might be inherited or arise as a de novo mutation. In case of genetic inheritance, both the alleles must be mutated in the gene [24]. When cancer arises, cells start to grow abnormally and escape apoptosis. Eventually the cancer mass grows to the point that it needs its own vasculature to support itself. This process is usually observed when cancer reach 1 or 2 mm^3 [25]. Moreover, Vascular Endothelial Grow Factor, VEGF is important in tumor angiogenesis and it has been found to be responsible for angiogenesis when found, even in small amounts, in stromal cells [26]. When the cancer mass is big enough [27] cancer cells detach (metastases) and spread to other regions of the body. Metastases, rather than primary tumor, are the main cause of deaths due to attack on vital organs [1, 3]. Figure 1 taken from Schroeder et al. [18] illustrate the metastasis pathway from primary tumor.

Figure 1

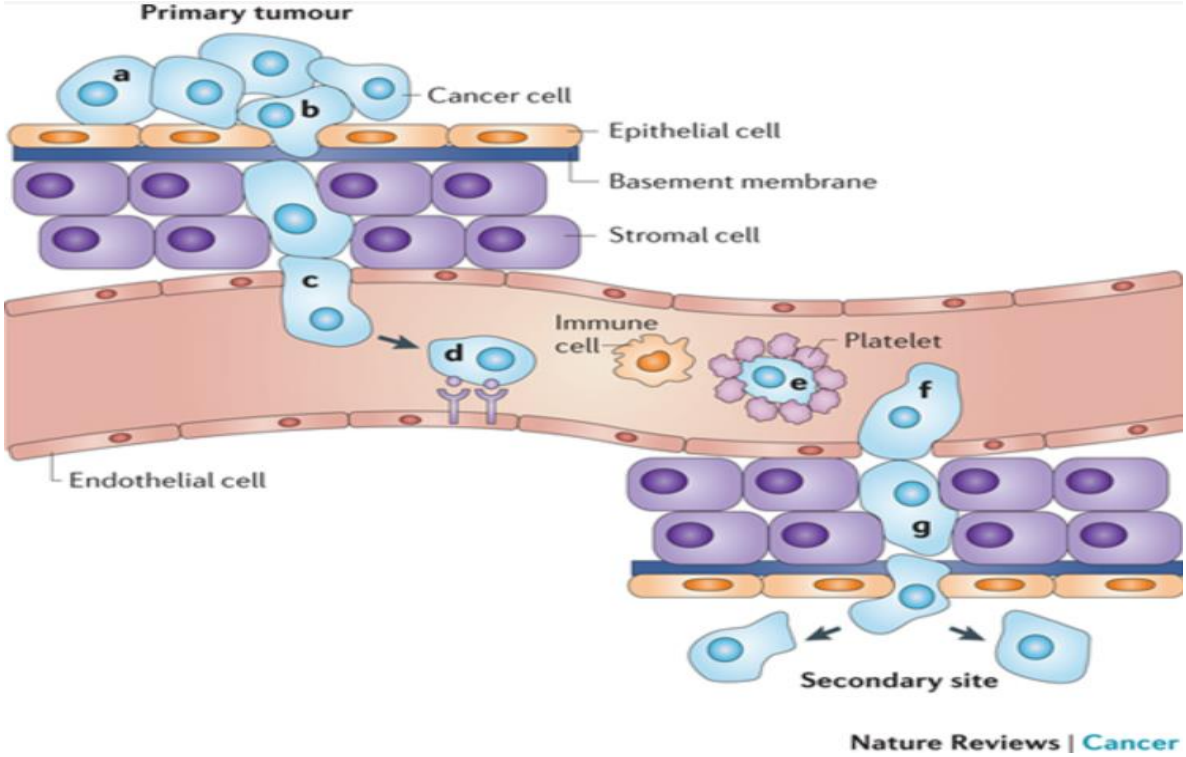

After detaching from the primary tumor by reducing adhesion (a) and clearing the path from neighbouring cells (b), cancerous cells enter the stroma. Subsequently, they can enter the blood stream in case of discontinuous vasculature otherwise cancer cells must cause either endothelial retraction by releasing VEGF or cell death by releasing metalloproteinases. After entering the blood stream cancer cells will distribute to other organs or tissues [18].

HUVEC

Human umbilical vein endothelial cells (HUVEC) well documented to express $\alpha_v\beta_3$ on their cell surface [13] and have been wide used as experimental in vitro models for studying the pathophysiological mechanisms of different diseases [14]. In particular, these cells have provided the ground for some major discoveries in molecular medicine, ranging from a better understanding in the pathophysiology of arteriosclerosis to the mechanisms regulating angiogenesis in tumor as well as hypoxia induced neovascularization [28-30]. The main reason HUVEC has been chosen for this study was the ability of expressing $\alpha_v\beta_3$ integrin.

$\alpha_v\beta_3$ integrin

The $\alpha_v\beta_3$ integrin is made of two genetically unrelated subunits a 125-kDa αv subunit and a 105-kDa β3 subunit [7]. This integrin can bind to a wide range of molecules that contain the RGD motif (Arginine - Glycine - Aspartic acid). This include fibronectin, fibrinogen, von Willebrand factor, vitronectin, and proteolysed forms of collagen and laminin [7, 8, 31].

$\alpha_v\beta_3$ integrin was identified as a marker of angiogenic vascular tissue [15], and appeared to be the most important of all the integrin [9]. Moreover, high expression of $\alpha_v\beta_3$ integrin on cancer vasculature has led to the interest in $\alpha_v\beta_3$ integrin for research of a suitable cancer-targeted drug delivery [7-9]. Targeting $\alpha_v\beta_3$ integrin with RGD conjugated peptides has been the focus of recent years in drug developments [7-9, 16-23].

Nanoemulsion

The use of nanoparticles offer several benefits in treating cancer compared to the traditional approaches. The increasing use on these novel technologies is part of the exciting trans-disciplinary field of nanomedicine, which includes disciplines such as chemistry, biology, medicine and physics to develop new nanotechnological approaches for biomedical applications [4-6]. Nanoparticles can be potentially used to deliver target specific drugs or as a contrast agent for molecular imaging [32]. Nanoparticles are various in size and compositions.

Nanoemulsion, particularly Oil-in-water nanoemulsion, are used throughout the experiments carried over in this study and consist of small oil droplets in water stabilised by a single layer of amphiphiles (chapter 4). Coating of the nanoemulsion is paramount for achieving the desired behaviour. The most extensively used type of coating, for all nanoparticles is PEGylation. The hydrophilic molecule polyethylene glycol (PEG) has been reported to both increase the nanoparticle half-life as well as improve the distribution of those to their targets [33, 34]. The most common method to functionalize the nanoparticle surfaces is to bind the peptides to the nanoparticle surface. These peptides are usually commercially available. Moreover, the surface of nanoparticles can be functionalised with target specific ligands or antibodies to achieve interaction only with the desired cells allowing specific drug delivery or imaging. For example by conjugating the RGD motif to the nanoemulsion surfaces targeted delivery to $\alpha_v\beta_3$ integrin can be achieved [19].

Exploiting the niche

Many researchers agree on the fact that understanding the cancer angiogenesis mechanics is key for fighting tumours [7-9]. In particular, there are two way nanoparticle can contribute in cancer therapy: passive diffusion in cancerous tissues due to the cancer specific EPR effect or targeted binding to cancer specific receptors. EPR effect stands for enhanced permeability and retention effect, which is the result of an abnormal rapid growth of blood vessels due to the increase of oxygen and nutrients demand form the tumor [25]. However, this rapid and growth of vasculature leads to chaotic and loosely connected endothelial cells as well as discontinuous basement membrane [35] which eventually leads to leaky blood vessels and constitute a portal for accumulation of nanoparticles in solid tumours [12]. Specifically, these openings in endothelial cells have been reported to range from 20 nm to approximately 2 μm while in non-tumorous vasculature may present gap openings smaller than 5 nm [10]. Therefore

nanoparticles bigger than 5 nm might accumulate in the tumour tissues while not affecting healthy vasculature [10].

The second method to achieve nanoparticles delivery to tumour tissues is to bind specific tumor targeting ligands to the nanoparticle surfaces, so that those nanoparticles would selectively bind on cancer specific biomolecules without affecting healthy cells [11]. Particularly in my study, the focus was selectively target the $\alpha_v\beta_3$ integrin with RGD conjugated nanoemulsion (RGD-NE) [7-9, 16-23] while using RAD conjugated nanoemulsion (RAD-NE) as a control because the latter doesn't bind to $\alpha_v\beta_3$ integrin [19].

Confocal Laser Scanning Microscope

Confocal laser scanning microscopy (CLSM) is a technique, which is widely used for the study of biological samples stained with fluorescent probes. The reason behind its popularity arises from the several advantages over a conventional widefield microscopy. First, confocal microscopy can eliminate the background light from samples which thickness is larger than the area of focus, thus enabling imaging of think biological slides with minimal background noise. Another key attribute of confocal imaging is its ability to capture optical sections of the samples. If these sections are stacked in a vertical manner it is possible to acquire a stacks (z-stacks) that can be rendered after in a three dimensional image. An additional advantage of using the CLSM is that fluorescent molecules can be detected even if they are smaller than the spatial resolution, allowing detection of very small features. Moreover, several fluorescent beads can be imaged at the same time and be detected separately to for individual images by using sequential scanning methods. The images from these channels can subsequently be arranged to form an overlay. Sequential scanning method allows for even less background noise for signal does not bleed through. Eventually the resolution and contrast of the images taken with CLSM can be adjusted by either lowering or increasing the magnification (zoom) and/or the scanning speed, a slower scanning speed results in higher resolution but require more time whereas higher magnification reduced the scanned area of the sample and the scanning rate.

Structure of the Confocal Laser Scanning Microscope

In the CLSM, the laser projector emits the light at a specific and adjustable excitation wavelength. This light passes through an adjustable pinhole, which is positioned in a confocal plane respect to the focal plane of the sample. After passing through the pinhole the light bounces and it is scattered by a dichromatic mirror and then it is converged by a lens to a small

focal volume in the focal plane of the sample where it excites the fluorophores. Subsequently the fluorescence emitted by the sample passes again through the lens and hit again the dichromatic mirror, this time the excitation wavelengths are blocked so that only the fluorescent emissions can pass through. A second pinhole is placed in the confocal plane before the detector so that out of focus fluorescent emission is blocked prior reaching the detector. However, fluorescence from the in focus planes are projected in the pinhole and registered by the detector. In order to achieve an image, the sample has to be scanned. Two high-speed oscillator mirrors positioned between the dichromatic mirror and the objective do this, particularly one mirror moves in the x direction while the other moves in the y-direction of the focal plane. Eventually, because the speed of these oscillator mirrors is slower compared to the speed of light, fluorescent emission will follow the same path as the excitation light back toward the dichromatic mirror [36]. Figure 2, illustrate a cartoon of the CLSM.

The only difference is that in my study the Detector used was a Hybrid detector rather than the photomultiplier detector. Hybrid detector technology surpassed the PMT technology in terms of images resolution [37] and was therefore preferred.

Figure 2

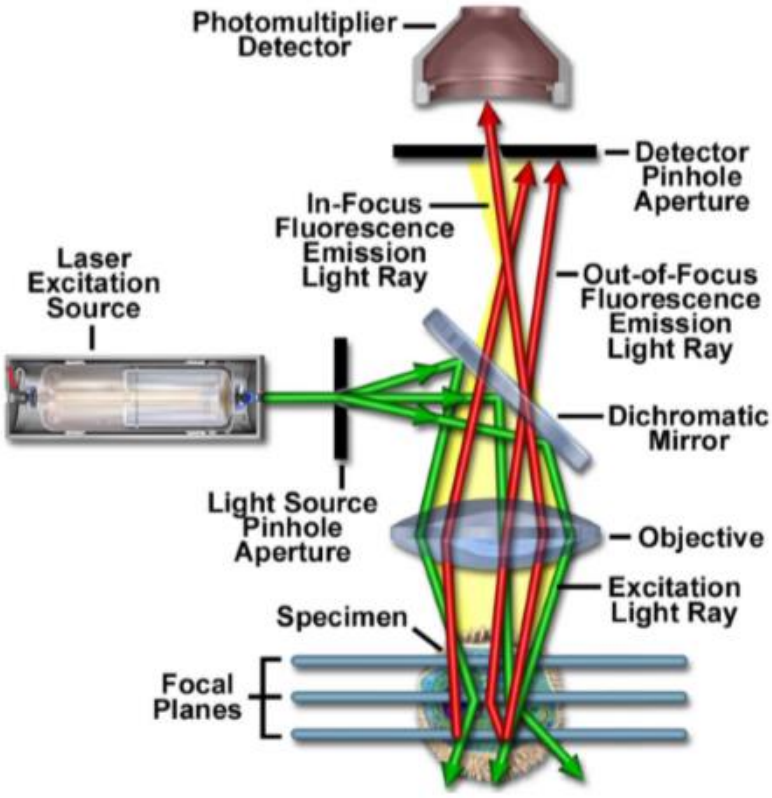

In this figure, the green arrows represent the excitation wavelength while the red arrow represents the fluorescent signal. Illustration for Claxon et al [36].

3 Materials

Nanoemulsions

The nanoemulsions used for the experiments were prepared in the Nano-lab cleanroom. The method used to produce nanoemulsions exploited the swift evaporation of organic solvents [38]. The core of the nanoemulsion was made of soya bean oil which was stabilized by 1,2-disteraoyl-sn-glycerol-3-phosphocholine (DSPC), cholesterol and 1,2-disteraoyl-sn-glycerol-3-phosphoethanolamine-N-[Maleimide(polyethylene glycol)-2000] (Mal-PEG-DSPE). The fluorophore used for CLSM detection was the L-α-Phosphatidylethanolamine-N-(Lissamine Rhodamine B Sulfonyl) (Rhodamine-PE). This fluorophore was incorporated in the emulsion membrane. The amphiphilic lipids and the fluorophore were acquired from Avanti® Polar Lipids, Inc. The fluorophore and lipids were weighted in vials and dissolved in chloroform at a molar ration of 62 : 33 : 5 (DSPC : cholesterol : Mal-PEG-DSPE). Soybean oil was weighted and dissolved in chloroform at a concentration of 2.6 mg/µmole of amphiphilic lipids. This process was carried out in a fume hood. Another pre-weighed vial containing 5 ml of HEPES Buffered Saline (HBS, 2.38 g/L HEPES and 8 g/L NaCl, pH 6.7) was placed under a fume hood on a heating and stirring device and the temperature was set to 70 °C. When the buffer reached the desired temperature, the lipids dissolved in chloroform were slowly dripped in the stirring solution. After the last droplet was added, the solution was let on the heater for additional two minutes before removing the stirring rod and weighting the vial. Then, distilled water was added to regain the total initial volume of 5 ml. The obtained emulsion was sonicated for 20 minutes (level 20 %, pulse 70 %, device: BioLogics, Inc., ultrasonic homogenizer model 150 V/T) with a thin sonicator tip (BioLogics, Inc., 3.9 mm) placed around 2-3 mm above the bottom of the glass vial to obtain nanoemulsion. The glass was placed in a in a water bath to keep room temperature. Eventually, nanoemulsions were stored until functional group conjugation. For experimental purposes, half of the nanoemulsions were conjugated with RGD peptide (c[-RGDf(-S-(acetylthio)acetyl)K-] while the rest was linked to the RAD peptide (c[-RADf(-S-(acetylthio)acetyl)K-] for control. Both RGD and RAD peptides were obtained from Peptides International. Prior to conjugation, the RGD peptide had to be exposed to a deacetylation buffer in order to be reactive. This buffer contained demineralized water, Hydroxylamine, HEPES, EDTA and NaOH tablets (all form Sigma-Aldrich®). The buffer pH was adjusted to 7. Next, 5 µl of buffer were added to an Eppendorf tube containing 50 µl RGD solution (2.5 mg/ml) and vortexed for one hour. Then, 6 µl of the solution was added per µmol of nanoemulsions and let

conjugate over night at 4 °C. The following day, nanoemulsion were dialysed in the Spectra/Por® Float-A-Lyzer® G2 (100 kDa molecular weight cut-off, Spectrum Laboratories) floating in HBS solution at pH of 7.4 to remove unconjugated RGD (719.82 Da) and salt from the buffer as well as obtaining pH close to physiological conditions. The floaters were set on the HBS while the solution was stirring in the cold room (4 °C). HBS was changed 3 times, approximately once per day, before the nanoemulsions were ready for experiments.

Stains

Two antibodies were used to tag the integrin. The primary antibody, mouse anti-integrin αvβ3, was purchased from Merck Millipore. This is a monoclonal antibody raised against the integrin $\alpha_v\beta_3$ receptor. The secondary antibody used was AlexaFluor488 goat anti-mouse IgG (Life Technologies), which was raised against the primary antibody and conjugated to the Alexa Fluorr 488® fluorophore for imaging.

The dye used to stain the plasma membrane was CellMask™ Deep Red Plasma membrane Stain from ThermoFisher. This plasma membrane stain contains amphipathic molecules, which anchor the probe in the plasma membrane.

CellMask™ plasma membrane staining pattern was also maintained after fixation with formaldehyde, which was key for the experiments, with the membrane staining being the last step before imaging after cell fixationn [39].

Fixation

The 4% Paraformaldehyde (PFA, Sigma-Aldrich®) solution in PBS and the methanol were prepared and stored in the freezer prior to the experiments.

4 Methods

Cell culture

HUVEC culture protocols include cell thawing, splitting and seeding routines. HUVEC cell line (Lonza Biosciences) was prepared by the staff engineer Kristin Sæterbø and frozen in liquid nitrogen at the IV passage containing approximately 1 million cells. The vial was thawed from liquid nitrogen by placing it in a glove sprayed with 70% ethanol in water solution and immersed in the water bath at 37 °C. Subsequently the vial was transferred in a safety level II laminar airflow cabinet (LAF) and sprayed again with 70% ethanol solution. Cells were then transferred to a TC 75 flask containing 15 ml of warm medium and incubated at 37 °C overnight. The medium used throughout the experiment was the endothelial cell basal medium-2 (EBM-2, Lonza, Clonetics) containing the EGM™-2 BulletKit™ (Lonza). In particular, this supplement was made of hEGF, Hydrocortisone, GA-1000 (Gentamicin, Amphotericin-B), FBS (Fetal Bovine Serum) 10 ml, VEGF, hFGF-B, R3-IGF-1, Ascorbic Acid and Heparin. The following day the medium was changed to remove traces of DMSO used for deep-freezing the HUVEC cells, by simply suctioning the old medium and replenish the TC 75 with 15 ml of warm medium. The flask was then placed in the incubator and cells were let to grow for 2 days before splitting to allow them to reach plateau. Cells were split when confluence was reached. After suctioning the medium and washing the flask with 5 ml warm PBS (Sigma-Aldrich®), cells were detached by using 3 ml of warm Trypsin/EDTA (Sigma-Aldrich®), solution (0.25%/0.02%) and incubated for 3 minutes. To monitor cell detachment, the flask was observed with Leica DMIL light microscope and gently shook when necessary. Next, 10 ml of warm medium was added to the flask to stop the trypsinizing process and 12 ml were collected in a tube (Corningr, CentriStar™) and centrifuged for 5 min at 15000 rpm (Megafuge 1.0, Heraeus Instruments). The rest of the cells were counted by placing them on slides (Countess™ Cell Counting Chamber Slides) and processed with the Invitrogen Countess™ Automated Cell Counter. Supernatant medium was then suctioned from the centrifuge tube leaving only the cells pellet at the bottom, which were re-suspended with the addition of warm medium.

The amount of medium needed for the pellet resuspension was calculated according to the formula:

$$\frac{X \times 6}{300.000\ Cells/ml} = Y$$

Where X is the average of the cell counted and 6 represents the 12 ml of cell suspension in the centrifuge tube divided by 2 (trypan blue was not added when counting the cells for viability assay was irrelevant in this study). After resuspension, 1 ml (300.000 cells) was taken from that solution, seeded in a TC 75 containing 14 ml warm medium and incubated immediately. This process was repeated until the cells reached the 7th passage, after which the cell line was considered senile and discarded while a new vial was thawed.

The rest of the cell suspension was diluted in order to obtain a solution of 20.000 Cells per 300 µl (optimized conditions) according to the dilution formula:

$$C1 \times V1 = C2 \times V2$$

Where the C1 is 300.000 Cells/ml, and C2 is 20.000 Cells per 300 µl (optimized conditions). V2 is the volume of the medium needed per wells (depending on the size of the experiment) and finally V1 represents the ml necessary from the re-suspended pellet tube required to make a solution of 20.000 Cells per 300 µl in function of V2.

Therefore, the equation was as follows:

$$\frac{(C2 \times V2)}{C1} = V1$$

Once the desired solution was obtained, cells were pipetted in chamber slides (µ-Slide 8 Well, ibiTreat) and incubated for 2 days prior to experiments. Medium was changed in the TC 75 every 2 days and cells were split at least once per week.

Nanoemulsions were introduced to the chamber slides after two days of incubation to allow cells to reach 80-90% confluence. Half of the slides were exposed to RGD conjugated nanoemulsions while the rest were exposed to RAD conjugate ones as a control. The nanoemulsions were diluted with warm medium to the concentration of 0.5 mM prior to cell exposure. 100 µl of the solution was pipetted per well after the medium was suctioned from the latter. Cells were then incubated for 10 minutes to mimic the integrin recycling of the *in vivo* conditions [40]. After incubation, cells were washed with warm PBS for 2 minutes, three times to remove all the possible excess of nanoemulsions that would cause background noise.

Confocal Laser Scanning Microscope settings

All images were captured using the Leica sp8 confocal laser-scanning microscope using the water objective 25x. The laser used in the Leica was White Light Laser (WLL). Images were taken using the excitation wavelength at 505 nm for the integrin channel while for the nanoemulsions and the CellMask™ stain the wavelengths were kept respectively at 550 nm and 650 nm. Laser power was adjusted accordingly until saturation. For z-stacks, the zoom was set to 4x magnification units on the microscope and the hybrid detectors (HyD) were used for better definition [37]. All images were taken using sequential scanning methods to avoid bleedthrough of the signal from the different channels. The resolution in z-direction in z-stacks was set using the system-optimized option.

Point Spread Functions

Point spread functions were needed to deconvolve confocal images in order to increase image resolution. Point spread function algorithms were extracted by imaging the ThermoFisher, PS-Speck™ Microscope Point Source Kit (blue, green, orange and deep-red fluorescent beads). In particular, Z-stacks of these beads were taken in conditions as similar as possible to cell imaging. The beads used were the green, orange and deep red, for integrin stain, nanoemulsion and CellMask™ stain respectively. Beads were set on the chamber slides with the aid of a mounting medium and exposed to 300 µl of PBS to mimic the conditions in which the fixed cells were imaged. Then, the zoom was set at 4x magnification of the water 25x objective in the Leica sp8 and after setting the respective wavelengths (505 nm for green, 550 nm for orange and 650 nm for deep red) z-stacks of the beads were collected. Once finished imaging, the z-stacks .lif files were loaded in Amira® 6 and visualized with the OrthoProjection module. Then suitable beads, such as those that were clearly visible and not superimposed by others or in clusters, were selected by using the Projection Cursor module. This allowed pinpointing a bead in the 3D space by clicking on any of the planes. Successively, these selected points were stored in the Landmarks data object. Multiple beads were chosen with this method to get a better average. Subsequently, beads were resampled in order to extract the precise function, and finally the PSF was calculated with the Extract Point Spread Function module. The images were loaded and visualized with the OrthoProjections module. Then a resampling round was carried out (Resample module) so that the extracted beads PSF and the images would have the same voxel size. The purpose of this was to feed the deconvolution module more accurate information. Eventually, images were deconvolved by connecting the Deconvolution module.

Optimization of the experimental conditions

Many experiments were carried out in order to optimize the reagents concentration as well as incubation time HUVEC were exposed to. This subsection presents the different experimental conditions used to optimize these variables.

Optimization of seeding density

Several protocols were used to determine which concentration of cell was optimal for the experimental conditions. Cells were first seeded in the chamber slides at the concentration of 5000 Cells/300 µl of medium per well. The amount was subsequently raised to 10.000 cells per well in 300 µl medium. Cell plating efficiency appeared to be dependable on the experimental conditions as well as senescence. In order to make them more resilient to detachment, gel pre-coating of the well plates was introduced to enhance cell adhesion and proliferation. This gel was made of porcine skin (Sigma-Aldrich®) and it was diluted to a 1% solution in warm PBS (57 °C). 200 µl were pipetted on each wells of the slides. Then, the slides were incubated at 37 °C for 30 minutes. After the incubation, the gel was suctioned and the slides were washed three times with warm PBS. Cells were seeded immediately to prevent gel desiccation. In case seeding was not possible, slides were wrapped in parafilm after 300 µl PBS was added to the well and stored in the refrigerator until usage.

Optimization of Fixation

Cells were initially fixed with 4% PFA in PBS at room temperature for 15 minutes but loss of cells was constantly reported after fixation. Therefore, several experiments were set to optimize the fixation procedure including both temperature variables, cell exposure time as well as using methanol. In particular, some chamber slides were set on ice, some were incubated at 37 °C and others were left at room temperature. A summary of these experiments is presented in Table 1. In addition, the concentration of the PFA was altered in different wells by diluting the initial 4% with PBS to obtain a solution of 3%, 2% and 1% PFA in PBS concentration. Data obtained by these three variables (time, condition of incubation and concentration of the PFA) helped to determine the best fixation protocol for HUVEC cells exposed to nanoemulsions.

Table 1

Incubation Time (minutes)	37 °C	RT	0 °C	-20 °C
15	PFA	PFA	PFA	
10	PFA	PFA	PFA	
5	PFA	PFA	PFA	methanol
2.5				methanol

This table enlists all experiments carried out in order to establish a suitable fixation protocol for HUVEC. In the first column is presented the incubation time, and in the successive rows and column the chemicals used for the experiment as well as the temperatures are shown. RT stands for room temperature

Optimization of Integrin staining

Optimization of the integrin staining was very straightforward. After fixation and washing, cells were placed on ice for two minutes and then exposed to 300 µl ice cold 1% Bovine Serum Albumin (BSA, Sigma-Aldrich®) in PBS for 5 minutes. Next, cells were incubated for 45 minutes at 37 °C with 80 µl of primary antibody, mouse anti-integrin αvβ3. Two different concentration of the antibody were tested, respectively 0.3 µg/ml and 1 µg/ml.

After the first incubation and the µ-wells were washed 3 times for 5 minutes in ice with 300 µl of 1% BSA in PBS. Then, cells were exposed to 80 µl of secondary antibody AlexaFluor488® goat anti-mouse IgG at a concentration of 0.5 µg/ml ice cold 1% BSA in PBS and incubated for 30 minutes at 37 °C. Eventually the plates were washed again three times for 5 minutes in ice with 300 µl of 1% BSA in PBS before CellMask™ stain.

Optimization of CellMask™ stain

Several experiments were attempted in order to optimize the CellMask™ stain. Remarkably, different protocols were tried on both live and fixed cells. It was later decided to stain cells as the last step of the experiment. Fixed cells were exposed to various concentration of CellMask™ solution in PBS for different time and let incubate at room temperature. The amount of solution per well was 150 µl. The amount of time of Cell mask exposure as well as incubation concentration in the various experiment is listed in Table 2. After CellMask™ incubation, wells were washed with 300 µl PBS for 2 minutes three times, then additional 300µl of PBS was pipetted in the wells and cells were imaged immediately with the Leica SP8 CLSM.

Table 2

Incubation Time (minutes)	CellMask™ Concentrations		
4	3 µg/ml	2 µg/ml	1 µg/ml
3	3 µg/ml	2 µg/ml	1 µg/ml
2	3 µg/ml	2 µg/ml	1 µg/ml
1	3 µg/ml	2 µg/ml	1 µg/ml

This table shows the different concentration of CellMask™ as well as incubation times that the fixed cells were exposed to.

Studies on colocalization

In order to study colocalization between $\alpha_v\beta_3$ integrin and RGD-NE the Fiji application was used [41]. After selecting and extracting the appropriate pictures from both the integrin and the nanoemulsion channels in the z-stacks and removing the eventual background noise, these images were analysed with the Fiji plug-in Coloc2, to quantify colocalization [42]. This plug-in provided multiple algorithms for analyses. Particular focus was set on the Manders Colocalization Coefficients especially the tM1 and the tM2, the threshold values of these colocalization coefficients [43]. These coefficients provide the ratio of the signal in one channel colocalizing with signal in the other channel ranging from 0 to 1, where 1 equals to total colocalization and 0 is random distribution [44].

Studies on internalization patterns, 3D

The 3D rendering were obtained through Amira® by processing the z-stacks taken from optimized experiments. The main method used for rendering was the Isosurface module. Images were deconvolved to define further details and to be as precise as possible

5 Results

This part is divided in two subsections. In the first subsection are presented the results obtained from the optimization experiments while the second one shows the results of the colocalization studies between $\alpha_v\beta_3$ integrin and RGD-NE as well as the studies on nanoemulsion internalization patterns over time.

Optimization of seeding density

The aim of the seeding density optimization experiments was to find a good protocol for cell seeding, to cope with cell detachment and loss after reagents exposure. From these experiments, it was found that cells were more prone to detachment when seeded in low concentrations. Although this could be avoided to some extent by seeding cells in chamber slides pre-coated with 1% gelatine solution, it was found that by increasing the cell concentration to 20.000 cells per 300 µl the gel coating was not needed altogether (Figure 3). No difference in cell plating efficiency was registered between the gel-exposed wells and non-exposed ones as it can be seen from Figure 3.

Figure 3

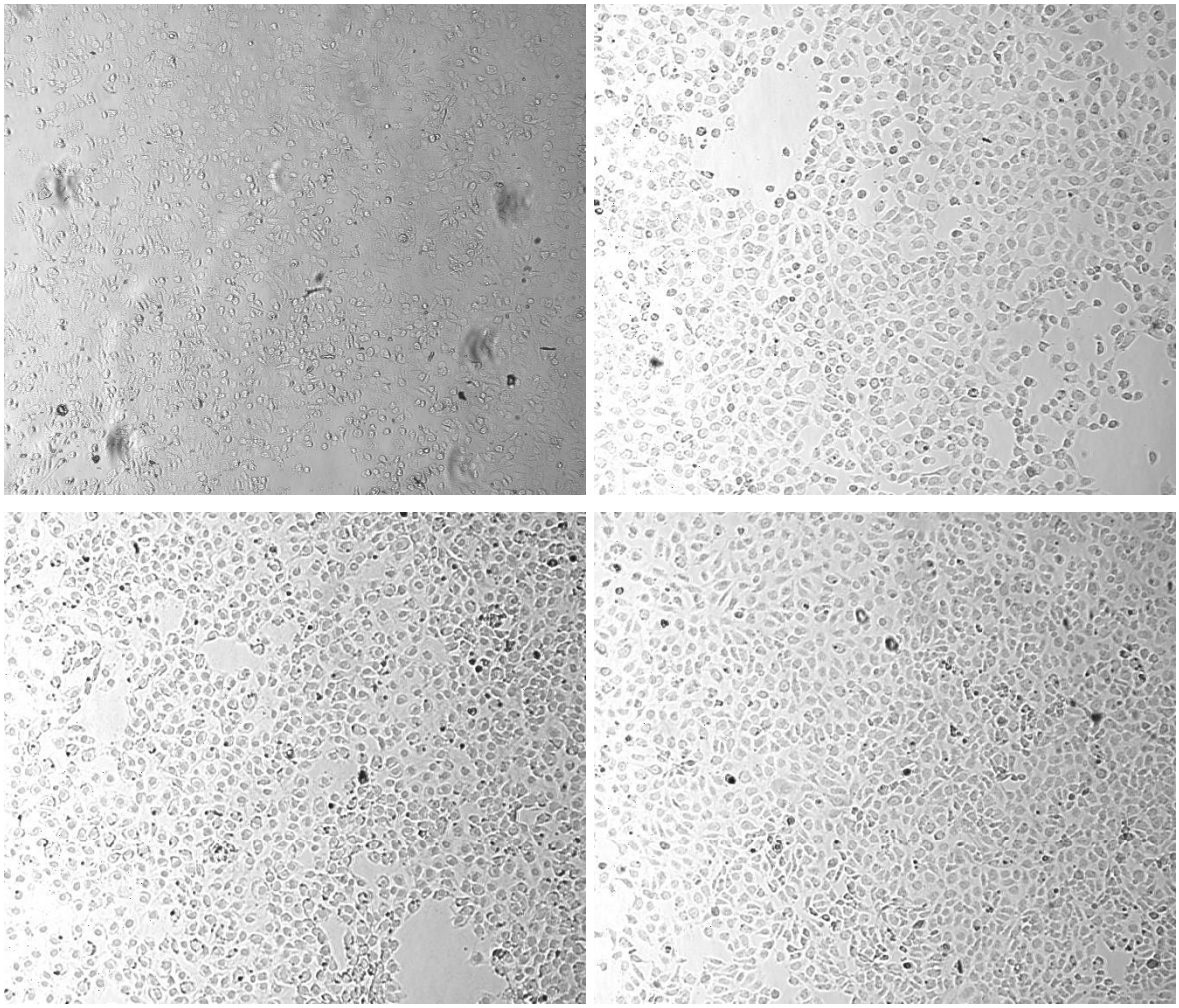

This figure reports the brightfield picture of HUVEC taken before and after experimental conditions. The experiments included nanoemulsion incubation (RGD-NE, 10 minutes 37 °C), fixation (300 µl per well for 5 minutes 3% PFA solution in PBS) integrin staining and finally CellMask™ stain. The pictures on the first row were captured prior to the experiments while the ones in the bottom rows are taken post reagents exposure. The pictures in the first column show the cells seeded in a gel-coated µ-well while the picture on the right column are cells seeded in non-treated µ-wells.

The experiment represented by Figure 3 opened up the possibility of trying to seed cells at high concentration without gelatine pre coating. This led to the experiment described in Figure 4

Figure 4

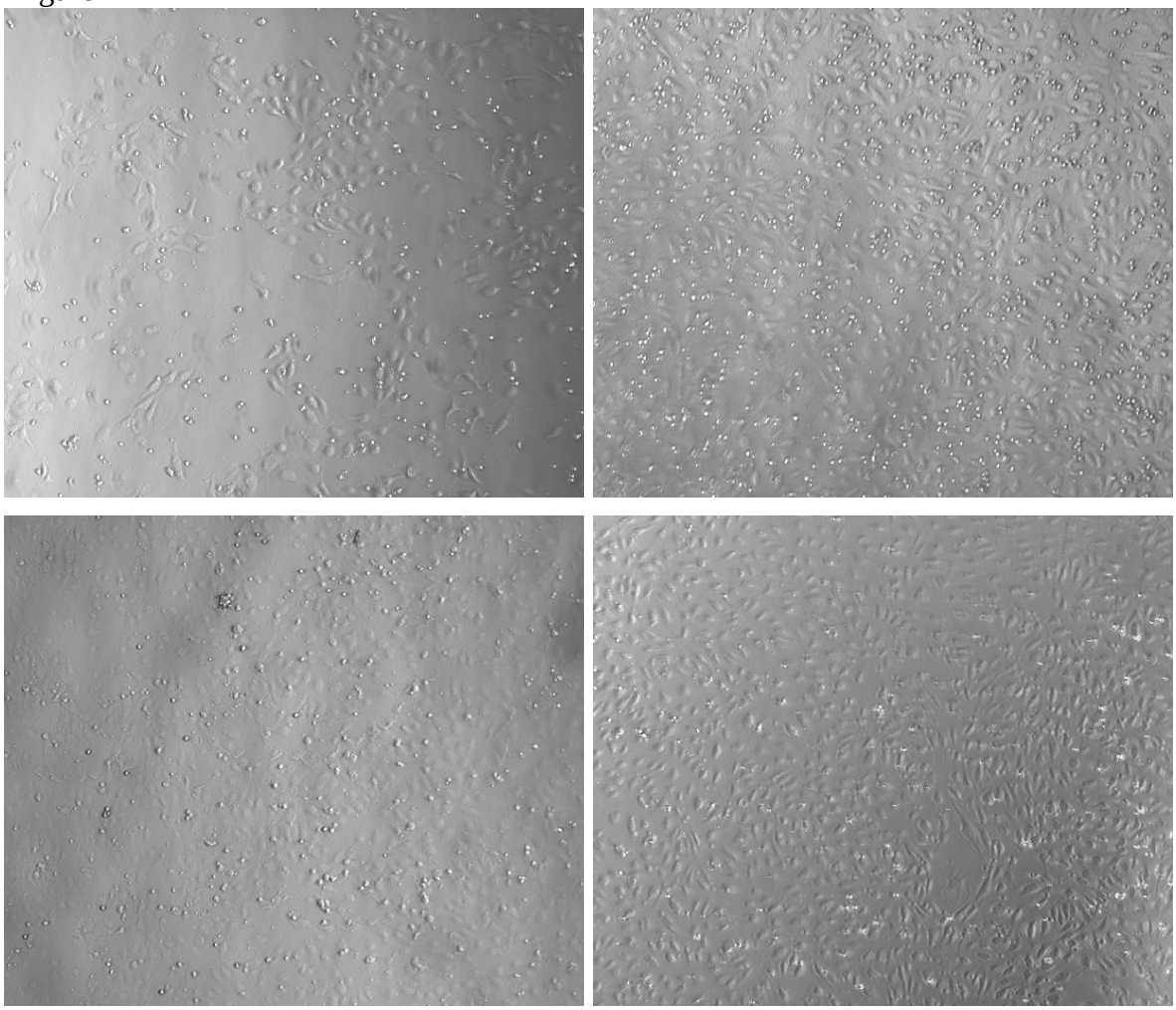

This figure reports the brightfield picture of HUVEC taken from different non-treated chamber slides seeded with 20.000 cells per 300 µl. The top row shows the pictures taken prior to experimental condition, while the second row shows the cells after nanoemulsion incubation (RGD-NE, 10 minutes 37 °C), fixation (300 µl per well for 5 minutes 3% PFA solution in PBS) integrin staining and finally CellMask™ stain.

From figure 4, is possible to observe that by seeding high concentration of cells per µ-well, the post-experimental cell concentration was satisfactory in terms of both cell plating and morphology, therefore the seeding density was kept at 20.000 cells per µ-well.

Optimization of Fixation

Although experiments with 200 µl of -20 °C methanol per µ-well both 5 minutes and 2.5 minutes were attempted for fixation, results were not satisfactory so the paraformaldehyde fixation route was preferred. After running the several optimization protocols described in section 4 it has been found that HUVEC responded the best, in terms of total cell density as well as morphology, when fixed for 5 minutes with 3% PFA solution in PBS at room temperature. Figure 5 shows an example of different fixation protocols.

Figure 5

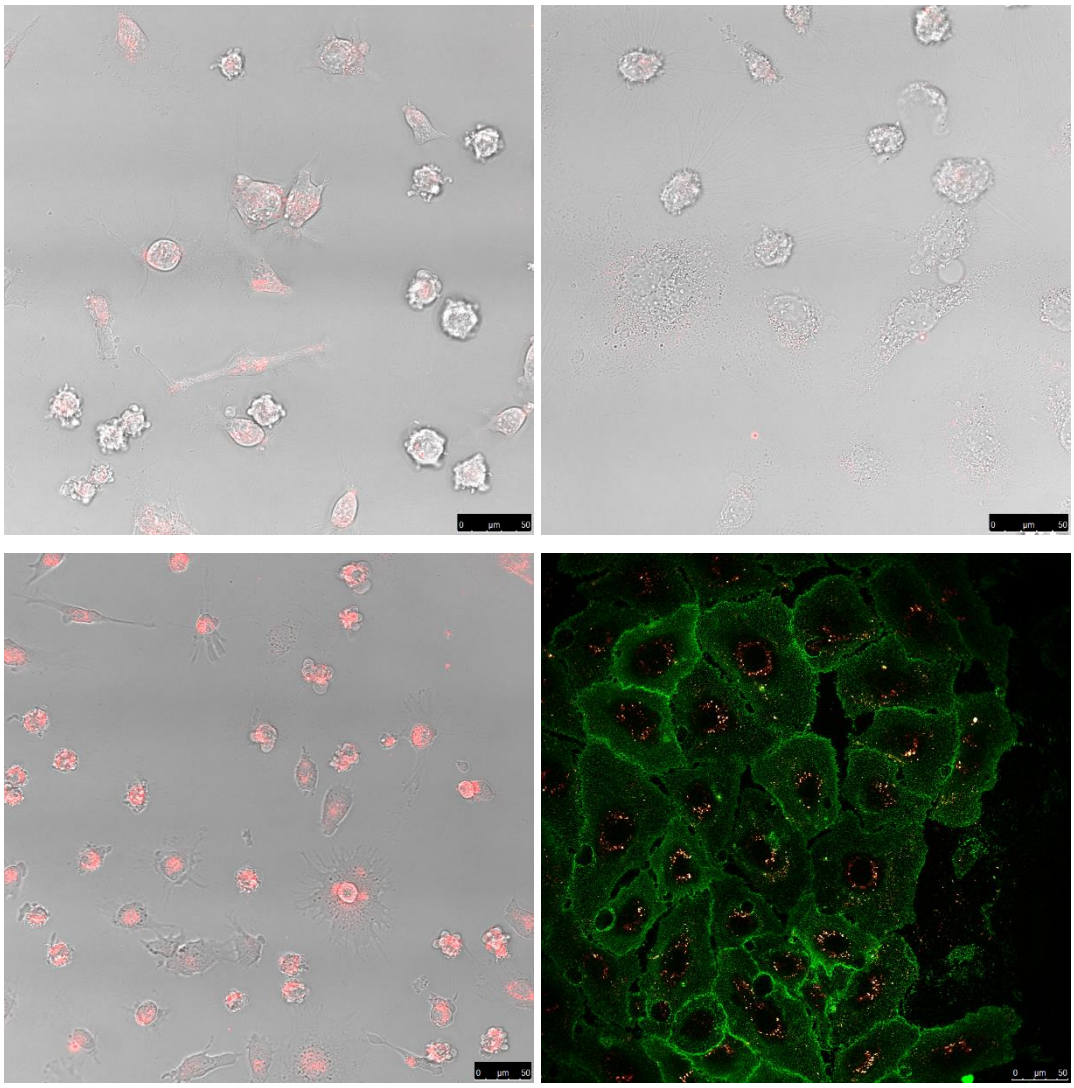

This figure show pictures overlay between brightfield and RGD-NE channel (first three pictures) and $\alpha_v\beta_3$ integrin and RGD-NE channel. From left to right pictures represent cells incubated with of 300 µl of 4% PFA for 15 minutes at 37 °C, 0 °C and room temperature. The last image represent cells fixed for 5 minutes with 3% PFA solution in PBS at room temperature.

The difference in cell morphology between non-optimized (brightfield + RGD-NE overlay) and optimized condition ($\alpha_v\beta_3$ integrin and RGD-NE overlay) was striking. Rounding up and ruffling of cell membrane, is especially evident in the first two images where the temperature of incubation was altered. Although, temperature was more or less the same of the optimized conditions (Room Temperature may vary slightly) cells in the third picture still showed signs of detachment and necrosis.

Optimization of Integrin staining

Results from the integrin stain experiments showed that the $\alpha_v\beta_3$ integrin was better labelled when tagged with the primary antibody (mouse anti-integrin $\alpha_v\beta_3$) at the concentration of 1 µg/ml. In Figure 6, it is possible to observe the changes in staining patterns as well as the signal intensity when feeding the cells with a lower concentration of primary antibody compared to the optimal one

Figure 6

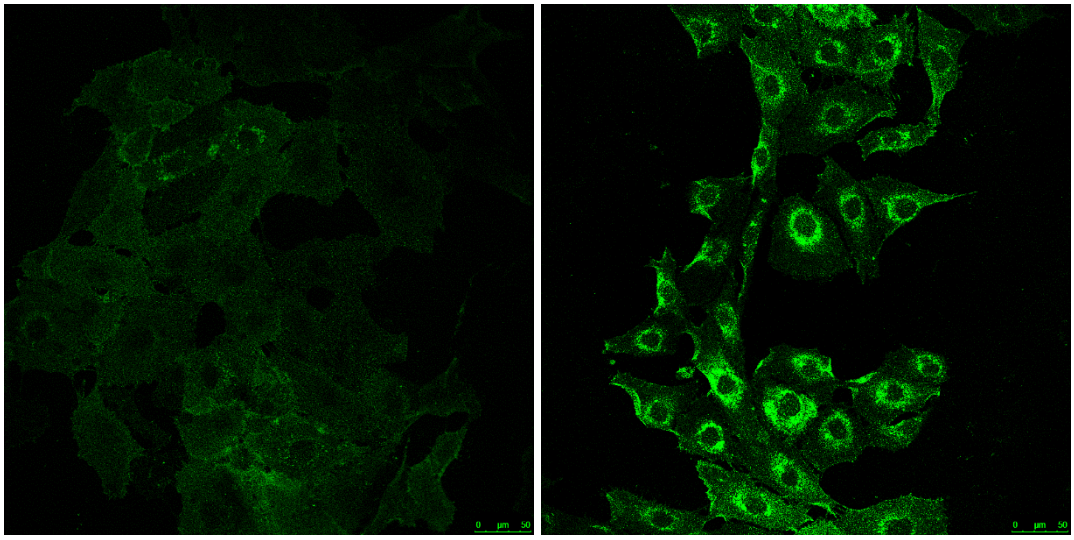

This figure presents a comparison between HUVEC cells stained with different concentration of with mouse anti-integrin $\alpha_v\beta_3$ (green). In the left cells were stained with 0.3 µg/ml while on the right with 1 µg/ml. By observing these images, it is possible to note the intensity as well as the staining pattern difference between the two experiments.

Optimization of CellMask™ stain

CellMask™ was attempted on both live and fixed cells, but it was later decided to leave the membrane staining as the last step of the optimized experiment prior to imaging to avoid cell membrane disruption. During these experiments, it was found that cells have been responding best when introduced to the CellMask™ in PBS solution at 2 µg/ml for 4 minutes at room temperature. When cells were exposed for less time, the stain appeared to be less strong on cells causing the cell membrane to appear almost transparent. From figure 7, it is possible to observe the difference between stains from cells incubated for different time points with 150 µl of 2 µg/ml CellMask™ in PBS solution. During the optimization process, the 1 and 2 minutes time points were discarded because the stain was weak after such a short incubation time. It was although more difficult to choose between the 3 and 4 minutes time point for the best one. Figure 8 and 9, show the images taken from cells incubated for 3 and 4 minutes respectively with CellMask™. From these images, it is possible to note how similar the stain was between the two time points, however, the 4 minutes time point was preferred for the slightly better stain as well as easy management during experimental procedures, which was ultimately an advantage when managing multiple µ-well slides.

The figures presented below were obtained both with the Leica sp8 (Figure 8 and 9) and with Amira® (Figure 7). In these figures, the integrin emissions are registered in green, the nanoemulsions are shown in red, and the CellMask™ stain is presented in blue.

Figure 7

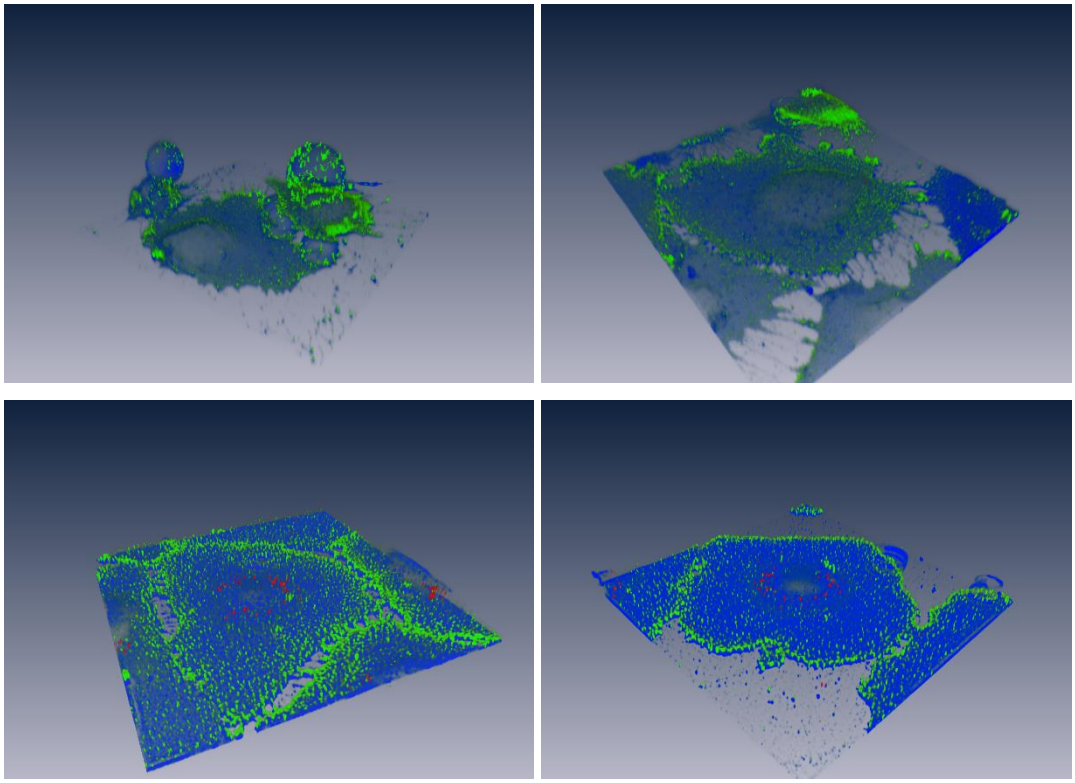

This figure represent the 3D rendering of HUVEC exposed to different incubation time of 150 µl of Cellmask™ at the concentration of 2 µg/ml after fixation. From top to bottom, left to right, exposure time varied of 1, 2, 3 and 4 minutes respectively.

Figure 8

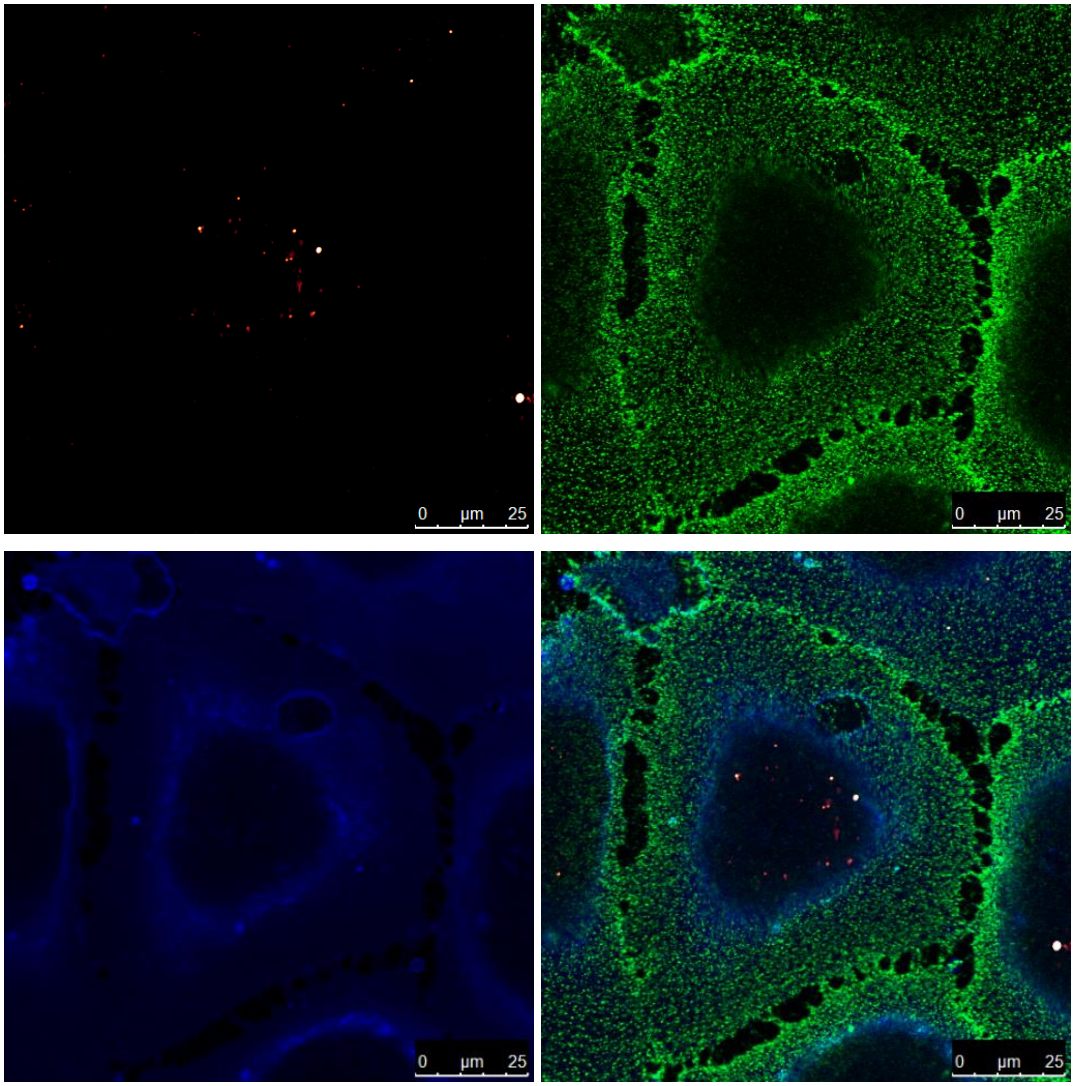

These images were taken with the Leica sp8. In particular, in the first picture represents the nanoemulsion channel, followed by the integrin channel, the CellMask™ stain channel and eventually the overlay of all above. These images were taken from a HUVEC cell incubated with RGD-NE for 10 minutes and successively re-incubated after washing for additional 30 minutes with medium. The CellMask™ incubation time was 3 minutes.

Figure 9

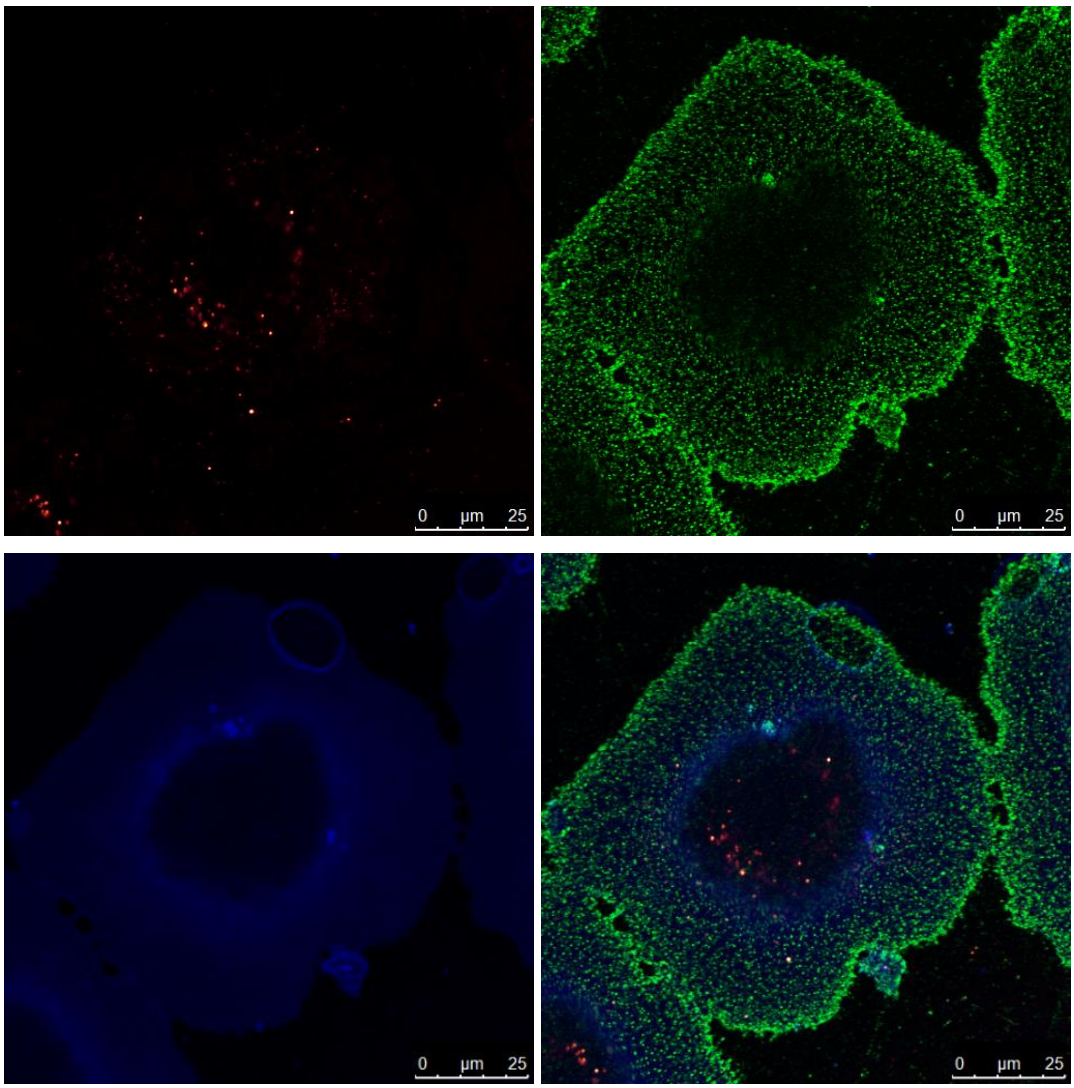

These images were taken with the Leica sp8. In particular, in the first picture represents the nanoemulsion channel, followed by the integrin channel, the CellMask™ stain channel and eventually the overlay of all above. These images were taken from a HUVEC cell incubated with RGD-NE for 10 minutes and successively re-incubated after washing for additional 30 minutes with medium. The CellMask™ incubation time was 4 minutes.

Optimized experimental conditions.

Optimal experimental condition were found to be when cells were seeded in the chamber slides at a concentration of 20.000 cells/300µl medium per well. Six chamber slides were used for the optimized experiment. Cells in three of them were exposed to RGD conjugated nanoemulsions while the other three were used for control and incubated with RAD conjugated nanoemulsions. Cells were subsequently incubated with medium for additional two days prior to the experiments so that they were at 80-90% confluence when prior to reagents exposure. On the experiment day medium was suctioned away and cells were exposed to 100 µl of nanoemulsion solution in medium at a concentration of 0.5 mM. Cells were then incubated for 10 minutes to mimic the integrin recycling of in vivo condition [40]. After incubation, cells were washed three times with 300 µl PBS for 2 minutes and some cells were fixed immediately by being exposed to 300 µl of 3% PFA in PBS solution for five minutes at room temperature. The rest was reintroduced to 300 µl medium and re-incubated for respectively 15 and 30 minutes prior to fixation. After fixation, both plates were washed three times with PBS for 2 minutes. Subsequently, cells were placed on ice for two minutes and then exposed to 300 µl ice cold 1% BSA in PBS for 5 additional minutes. Next, cells were incubated for 45 minutes with 80 µl of primary antibody (mouse anti-integrin αvβ3) at a concentration of 1 µg/100µl ice cold 1% BSA in PBS. After the first incubation and washing (3 times 5 minutes with 1% BSA in PBS) cells were exposed to 80 µl of secondary antibody (AlexaFluor488® goat anti-mouse IgG) at a concentration of 0.5 µg/100µl ice cold PBS with 1% BSA and the incubated for 30 minutes. Then, cells were imaged and z-stacks were collected. Eventually, cells were exposed to 150 µl of CellMask™ at a concentration of 2 µg/ml, and incubated at room temperature for 4 minutes to better assess the degree of interaction between integrin staining and nanoemulsions as well as investigating the nanoemulsions distribution inside the cells in function of time. This protocol was used both for colocalization studies and for nanoemulsion internalization pattern studies. Table 3 summarizes the results found to work best with HUVEC from each optimization experiment.

Table 3

Cells	20.000 Cells/300µl medium
Nanoemulsion (RGD or RAD)	100 µl of 0.5 mM (RGD/RAD) in medium
Incubation	10 minutes
Additional incubation in medium prior to fixation	0, 15, 30 minutes
Fixation protocol used	300 µl of 3% PFA in PBS solution for 5 minutes (room temperature)
Integrin staining (AB I)	80µl of 1 µg/100µl AB I (mouse anti-integrin αvβ3)
Integrin staining (AB II)	80µl of 0.5 µg/100µl AB II (AlexaFluor488® goat anti-mouse IgG)
CellMask™ Staining	150 µl of 2 µg/ml CellMask™ in PBS for 5 minutes (room temperature)

The table reports a summary of the optimized conditions as well as the amount and concentration of the reagents used during the experiment.

Studies on colocalization

In this experiment, we studied colocalization between the RGD-NE signal and the integrin stain signal. Three chamber slides were seeded with HUVEC, two of which were incubated with RGD-NE for 10 minutes and the remaining was left as control. One slide was fixed immediately while the other was re-incubated with medium for additional 30 minutes after washing.

Images of both conditions were taken by sequential scanning in the Leica sp8. First, the images from nanoemulsions and the integrin channels were observed to find evidences in clustering patterns of the integrin around the nanoemulsions by using an overlay of the channels (Figure 10). Some degree of colocalization might be observed from these images especially when analysing the overlay of the two channels. In particular, the yellow dots in the pictures were signs of signal colocalization. Subsequently, the images were investigated further by taking z-stacks of HUVEC at different time points 0 and 30 minutes of incubation in medium after 10 minutes of nanoemulsion exposure. These z-stacks were then processed with the Coloc2 plug-in of Fiji as stated previously. In Table 4, the results obtained by processing the images with the Coloc2 algorithm are summarized. Table 5 reports the average of the tM1 and the tM2 of both the time point as well as their sample standard deviation. By observing these tables, it was clear that the rate of colocalization between the integrin and the RGD-NE was very low in accordance to the images in Figure 10 and appeared to be independent of incubation time.

Figure 10

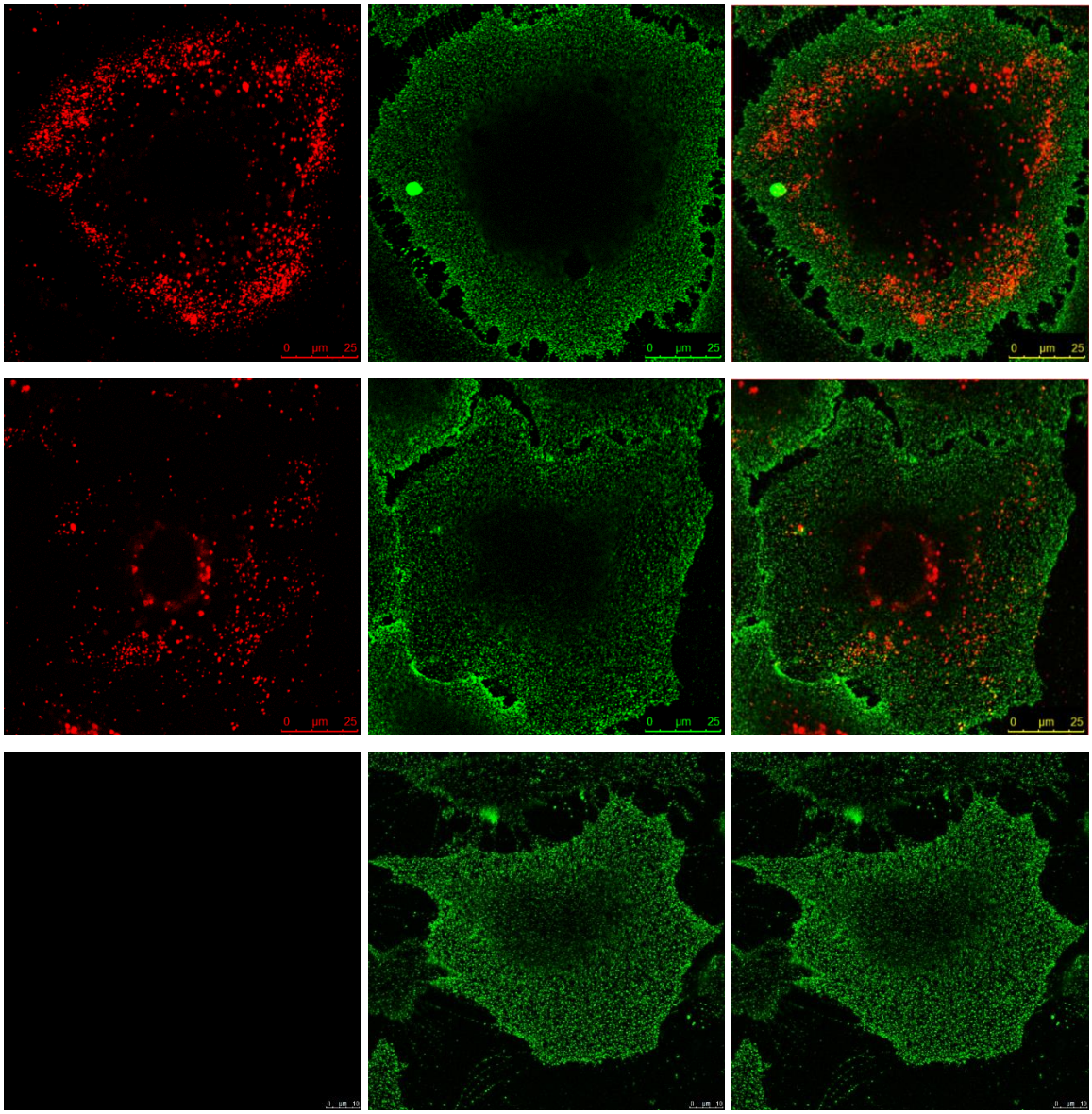

In this figure are presented the results from the CLSM images taken for the 0 minutes time point the 30 minutes time point as well as images of cells incubated only with the integrin stain as control, respectively the first, the second and the third row. The first column represents the RGD-NE signal, the second column shows the integrin signal channel and finally in the third column is an overlay of both the channels

Table 4

Time (min)	tM1	tM2	Time (min)	tM1	tM2
0	0.23	0.107	30	0.118	0.052
0	0.112	0.091	30	0.02	0.002
0	0.157	0.239	30	0.002	0.364
0	0.027	0.087	30	0.112	0.152
0	0.28	0.178	30	0.028	0.324
0	0.173	0.54	30	0.091	0.343
0	0.125	0.401	30	0.23	0.142
0	0.212	0.067	30	0.125	0.145
0	0.249	0.055	30	0.009	0.296
0	0.251	0.089	30	0.076	0.137

These tables summarize the results of the Manders analyses run on 20 cells, 10 fixed as soon as they finished incubating with RGD-Ne and 10 fixed after 30 minutes of additional incubation in medium.

Table 5

0 minutes	TM1	TM2
Average	*0.1816*	*0.1854*
StDev	*0.07812838*	*0.1633702*

30 minutes	TM1	TM2
Average	*0.0811*	*0.1957*
StDev	*0.07035379*	*0.12715786*

These tables represent the average and the sample standard deviation of both the Manders algorithms in the different time points.

Studies on nanoemulsion internalization patterns, 3D rendering analyses

This subchapter presents a comparison between the different 3D renderings in terms of nanoemulsion distribution patterns in HUVEC. These reconstructions were obtained 0, 15 and 30 minutes after fixation respectively. The fixation at the zero minute time point means that the cells were fixed after the 10 minutes nanoemulsion incubation (Figures 8, 9, 10, 11, 12 and 13). The 3D rendering were obtained through Amira®. Images presented below were taken from the "x, y" plane prospective and show respectively: the nanoemulsion rendering, the CellMask™ stain rendering, the rendering of the overlay of the two channels and finally a cross section of the cell membrane. The integrin channel (green) was excluded to avoid noise. The purpose of this was to observe the cell surface and therefore study the distribution of the nanoemulsions inside the cells in function of time and the difference in distribution patterns between RAD-NE and RGD-NE. The last two images were particularly useful because from them it was possible to extrapolate the nanoemulsions distribution inside the cell.

From these 3D renderings, patterns were observed in internalization of the different nanoemulsions. Particularly while in the cells incubated with RGD-NE the nanoemulsions were observed moving towards the perinuclear area over time (Figures 11, 13 and 15), the renderings from the cells exposed to RAD-NE showed a more random internalization behaviour of these nanoemulsions.

Figure 11

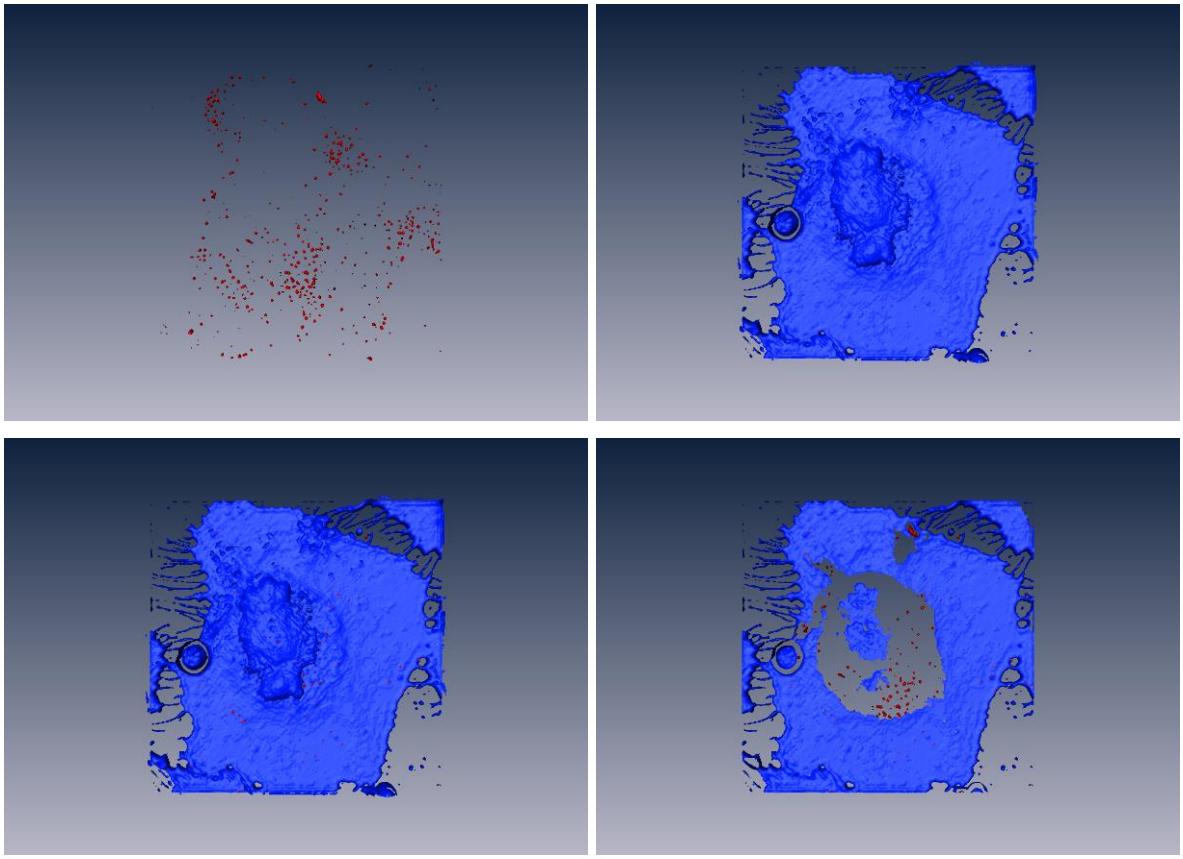

In this 3D rendering is represented a HUVEC cell fixed after 10 minutes of RGD-NE incubation without additional incubation and stained with CellMask™, 4 minutes exposure time.

Figure 12

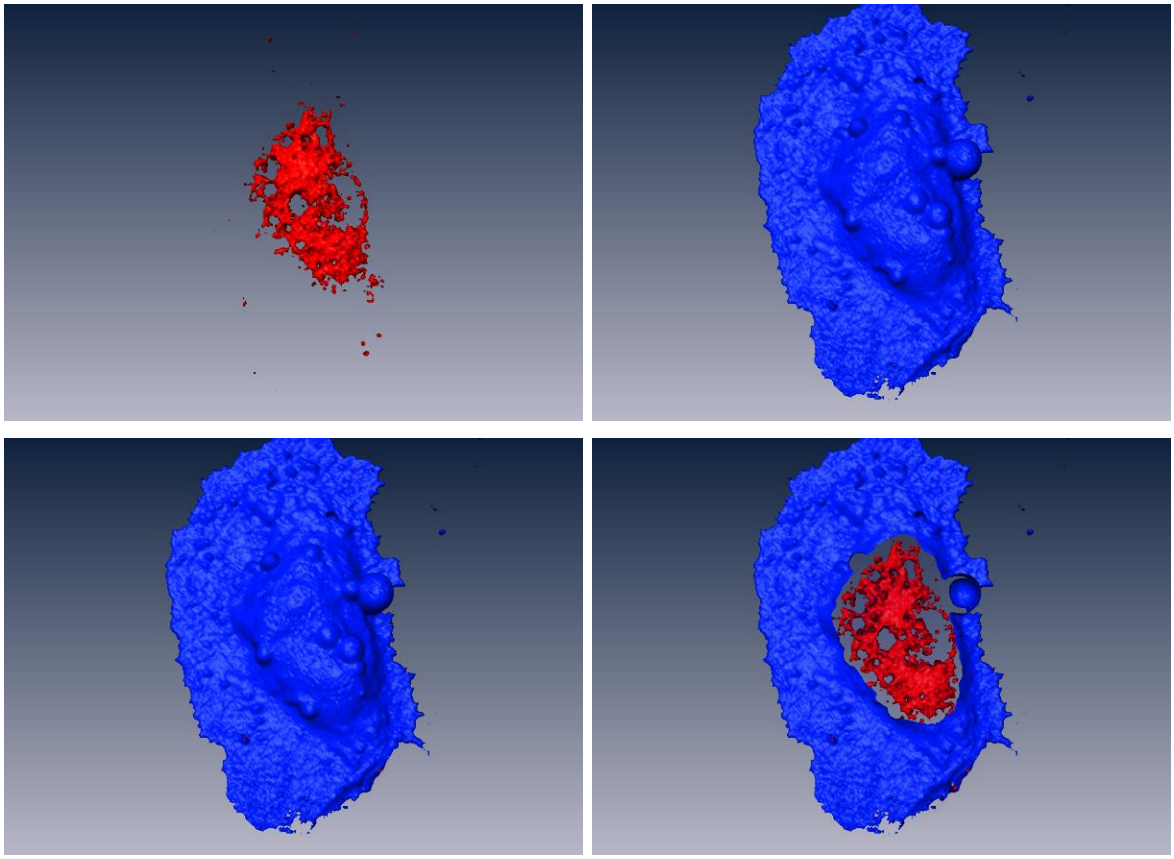

In this 3D rendering is represented a HUVEC cell fixed after 10 minutes of RAD-NE incubation without additional incubation and stained with CellMask™, 4 minutes exposure time.

Figure 13

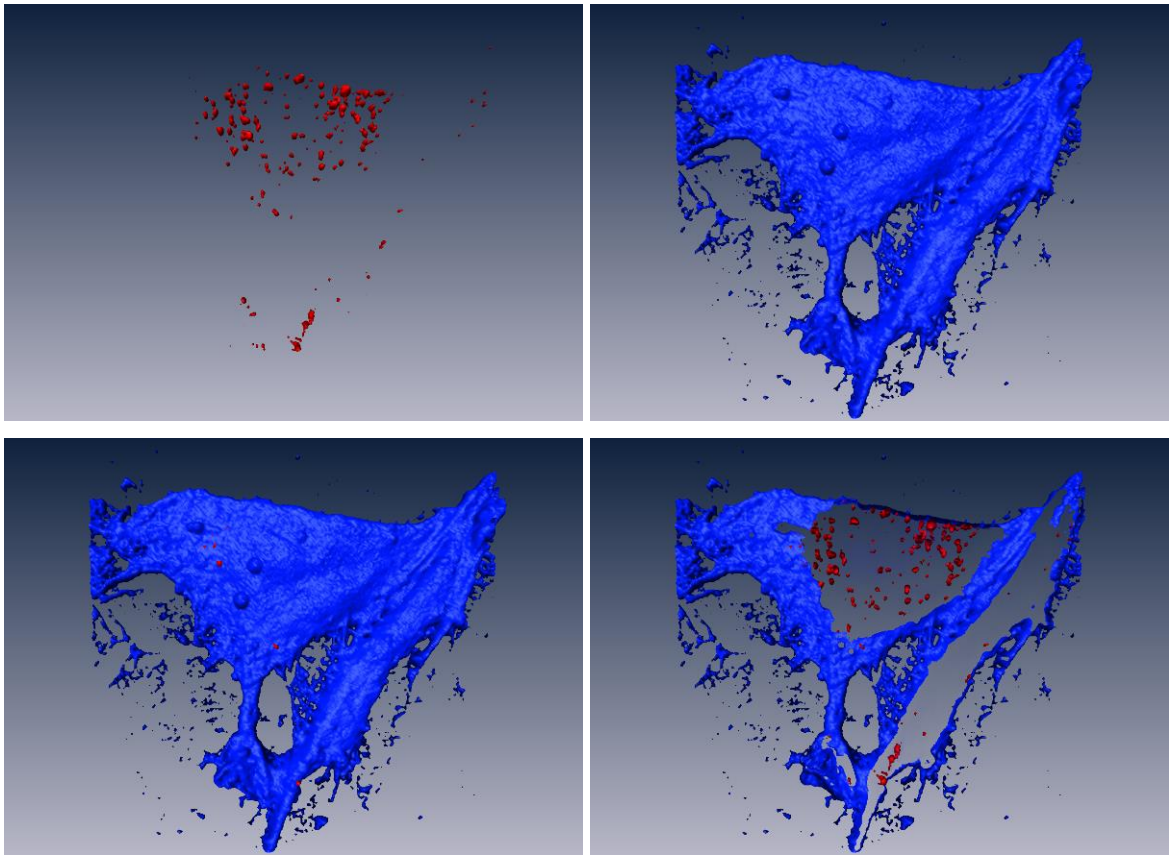

In this 3D rendering is represented a HUVEC cell fixed after 10 minutes of RGD-NE incubation with 15 minutes additional incubation and stained with CellMask™, 4 minutes exposure time.

Figure 14

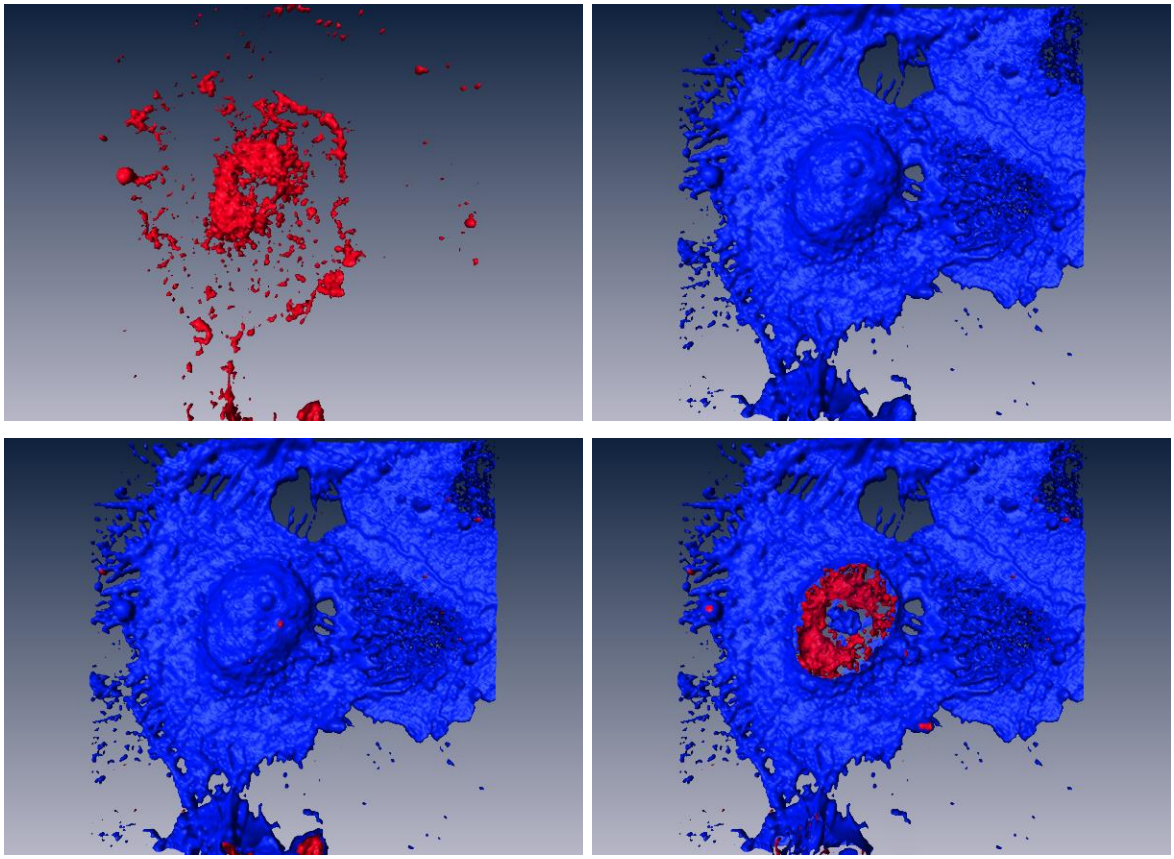

In this 3D rendering is represented a HUVEC cell fixed after 10 minutes of RAD-NE incubation with 15 minutes of additional incubation time and stained with CellMask™, 4 minutes exposure time.

Figure 15

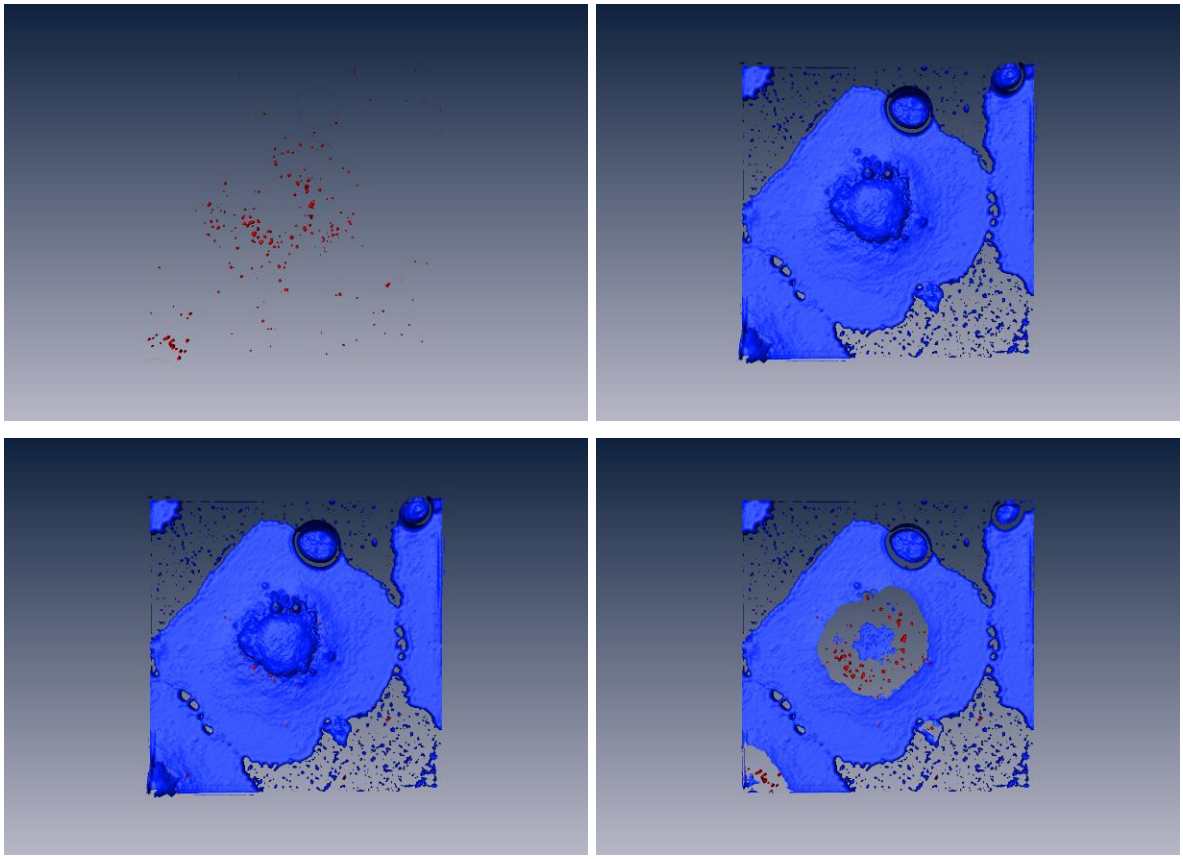

In this 3D rendering is represented a HUVEC cell fixed after 10 minutes of RGD-NE incubation with 30 minutes additional incubation and stained with CellMask™, 4 minutes exposure time.

Figure 16

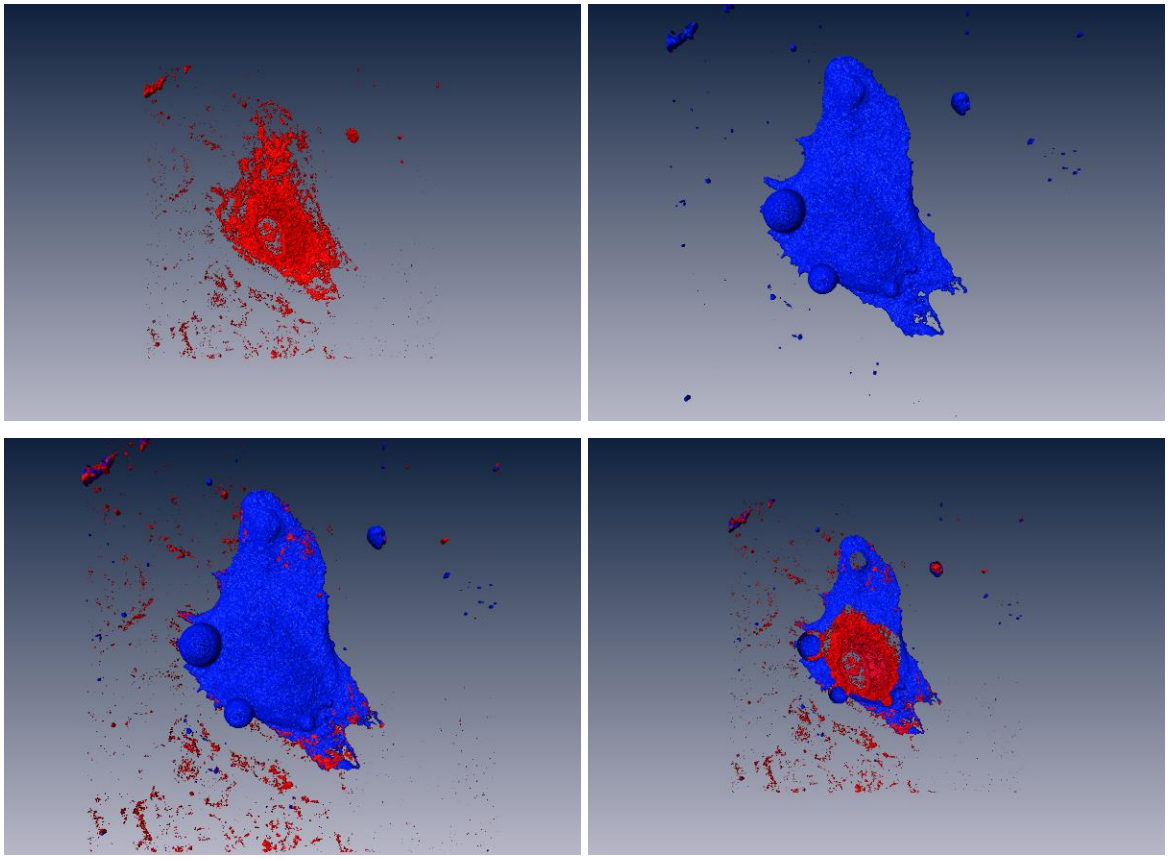

In this 3D rendering is represented a HUVEC cell fixed after 10 minutes of RAD-NE incubation with 30 minutes of additional incubation time and stained with CellMask™, 4 minutes exposure time.

Studies on nanoemulsion internalization patterns, ROI analyses

CLSM images were also analysed with Fiji in order to quantify the voxels of the nanoemulsions and to make a better claim for spatial distribution of these in function of time rather than just relying on 3D renderings. First, the channels in the z-stacks were split then suitable images were duplicated and extracted. Then, using the Fiji-ROI Manager plug-in, Regions of Interest (ROI) were traced in the cells outermost area in a ring fashion either on the integrin channel (Figure 17) or on the CellMask™ channel and then exported to the nanoemulsion channel. Next, an inner ROI was traced. Eventually the NE intensity in these, were measured with the ROI Manager plug-in and the data from the different time points is summarized in Table 6 and 7.

Figure 17

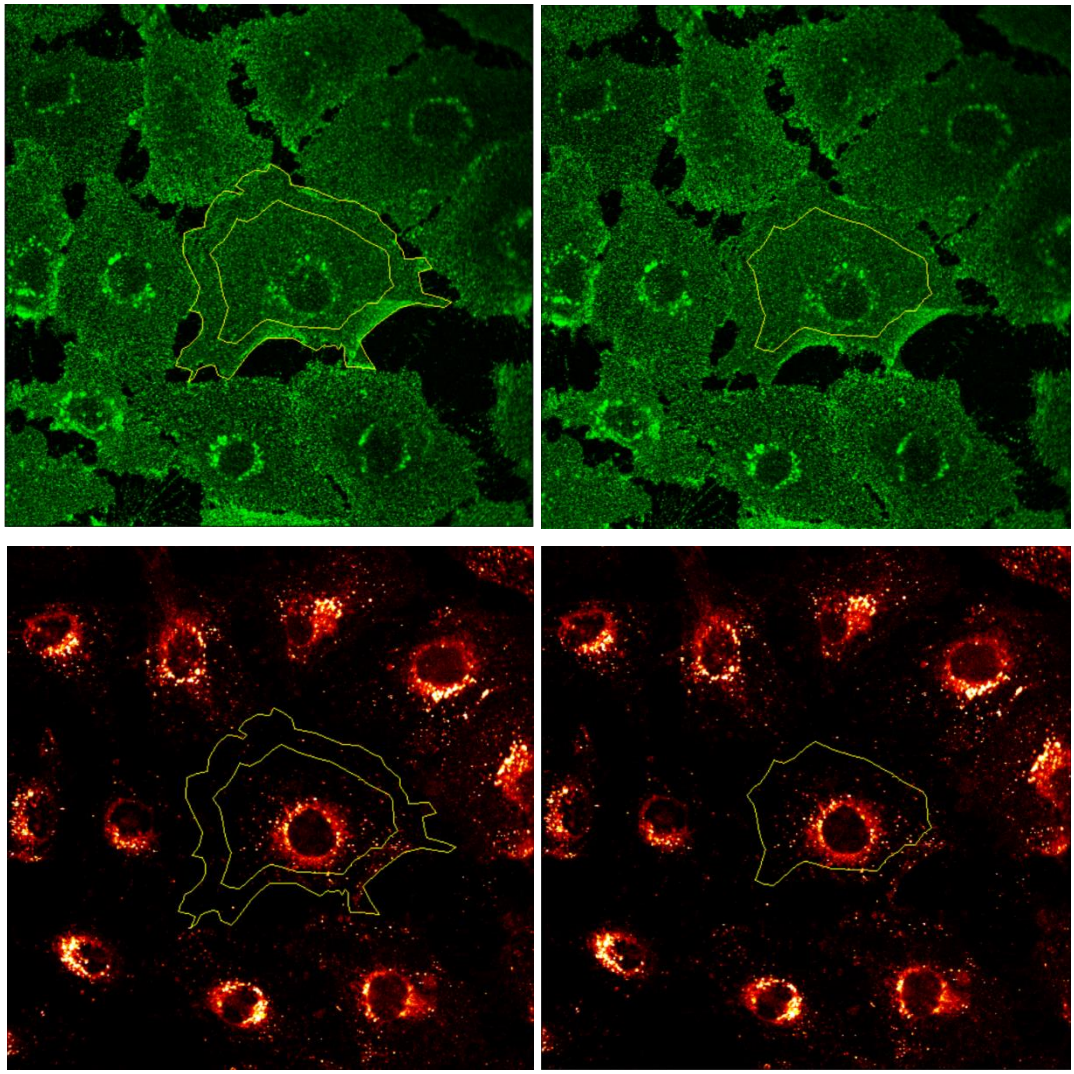

These images show how Regions of Interest were traced on cells. The cell silhouette was first traced on the green channel (integrin) and then an inner ring was drawn. The ROI was moved on the nanoparticle channel (in red) and the voxels were calculated using the plug-in. The same process was applied for the inner ring.

Table 6

RGD-NE

Time (minutes)	Outer voxels average	Inner voxels average
0	13.363	11.039
0	16.504	15.263
0	12.945	9.789
0	10.974	10.098
0	8.796	8.539
0	8.334	8.449
0	7.119	7.438
0	4.818	7.279
0	5.426	5.295
0	6.846	8.921

RAD-NE

Time (minutes)	Outer voxels average	Inner voxels average
0	28.068	28.47
0	28.757	30.048
0	23.491	21.24
0	25.2	24.588
0	27.535	28.886
0	29.235	29.08
0	28.024	32.081
0	6.329	6.221
0	30.927	28.189
0	13.828	15.439

RGD-NE

Time (minutes)	Outer voxels average	Inner voxels average
15	27.139	45.765
15	21.581	34.447
15	13.56	27.852
15	10.512	17.012
15	7.299	12.808
15	7.987	8.689
15	11.877	21.107
15	6.797	11.195
15	8.34	14.875
15	11.36	30.082

RAD-NE

Time (minutes)	Outer voxels average	Inner voxels average
15	31.356	30.24
15	7.319	11.071
15	9.052	12.309
15	11.011	11.094
15	11.585	10.477
15	11.84	12.299
15	10.761	11.333
15	9.91	10.591
15	13.348	11.213
15	12.622	12.488

RGD-NE			RAD-NE		
Time (minutes)	Outer voxels average	Inner voxels average	Time (minutes)	Outer voxels average	Inner voxels average
30	3.309	8.081	30	24.519	28.338
30	2.21	8.242	30	24.729	29.35
30	13.326	20.784	30	15.898	19.068
30	5.978	10.276	30	27.345	29.722
30	6.466	15.547	30	7.493	10.257
30	14.592	29.949	30	8.925	10.701
30	17.343	28.527	30	10.922	13.184
30	14.066	33.359	30	13.369	15.59
30	13.344	25.59	30	14.785	14.052
30	13.475	23.645	30	22.77	21.017

In these tables there are listed both the outermost and innermost voxels means calculated with Fiji-ROI manager for both RAD and RGD conjugated nanoemulsions in three different time points. In the first column, the additional incubation time is presented, while the second and third column show the outer and inner average voxel count respectively.

Table 7

RGD-NE	Inner mean	Outer mean	Ratio I/O	STDev
0	9.211	9.5125	0.96830486	0.22411579
15	22.3832	12.6452	1.77009458	0.39334693
30	20.4	10.4109	1.95948477	0.64134929

RAD-NE	Inner mean	Outer mean	Ratio I/O	STDev
0	24.4242	24.1394	1.01179814	0.07829317
15	13.3115	12.8804	1.03346946	0.20626094
30	19.1279	17.0755	1.1201956	0.13024513

In this table, is presented the average of the inner and outer voxel ratio of both RGD and RAD conjugated nanoemulsions from Table (6) and their respective sample standard deviation. These data were used to plot the graphs in Figure 18.

Figure 18

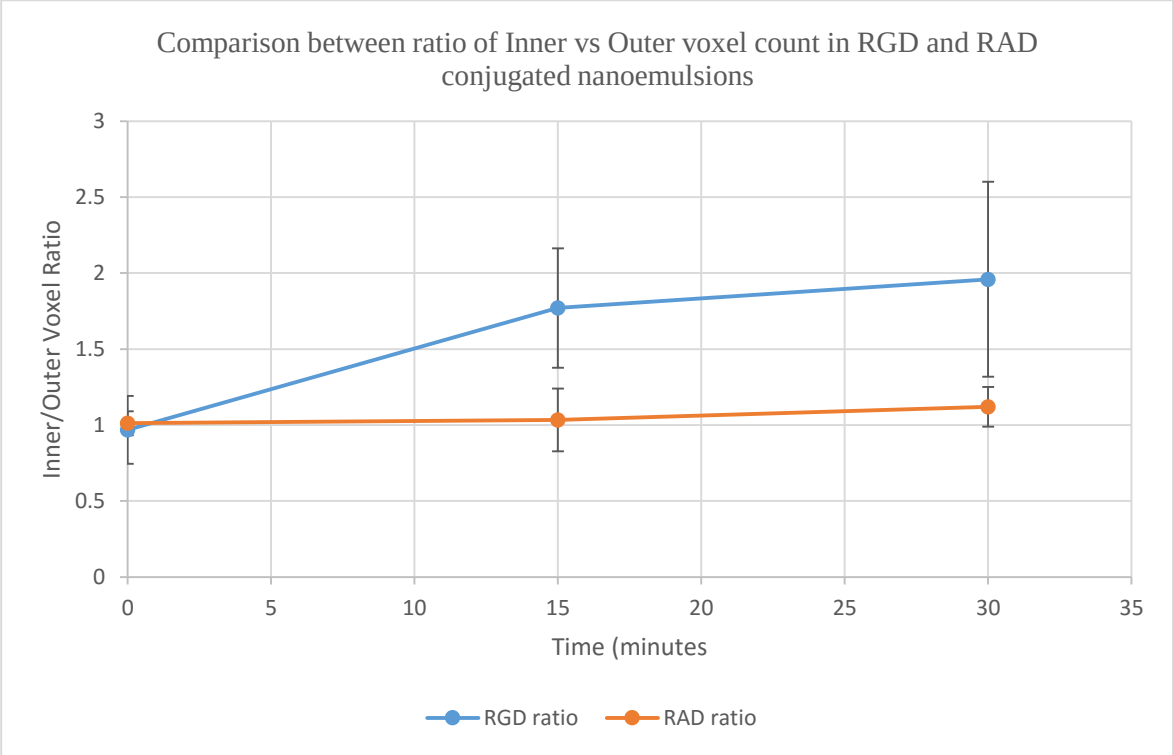

The graph visually represent the data from Table (7). In particular, the blue line shows the Inner/outer voxel ratio in cells exposed to RGD-NE over time while the orange line represents the inner/outer voxel ratio in cells exposed to RAD-NE.

From these results, it was possible to observe a change in internalization pattern of cells exposed to both RGD and RAD nanoemulsion by looking at the average of nanoemulsions found in the outer ring compared to those found to the inner ring over time. In particular, nanoemulsion distribution appears to be random in the 0 minutes time point for both RGD-NE and RAD-NE exposed cells because the mean voxels found is similar in both the outer and the inner rings. However, after 15 and 30 minutes of additional incubation time the signal from the RGD nanoemulsion found in the inner ring was significantly higher compared to the signal from the outermost part of the cells (Tables 7 and 8). In addition, while the inner/outer voxel ratio increased of almost two folds over time in cells exposed to RGD-NE the ratio of inner/outer voxels was not affected by additional incubation time in RAD-NE exposed cells (Figure 18).

6 Discussion

The first aim of this study was to find a good optimization protocol, which yielded the best results in terms of cell plating efficiency and cell density after the fixation, antibody tagging and membrane staining experiments on HUVEC incubated with nanoemulsion.

Studies on cell seeding density

From the results obtained by running several of seeding density experiment it was found that the best concentration for cell seeding was 20.000 cells per µ-well in 300 µl medium. Although, it was observed that density varied in accordance with both gel pre-coating of the µ-wells and senescence. In many studies researchers have seeded HUVEC with another cell line in co-cultures [45] while in others they adopted different kind of attachment substrates, to either mimic the in vivo conditions [46] or to enhance proliferation [47-49]. In a study carried out with HUVEC [14], optimal cell seeding density was investigated and it was found to be at 60.000 cells per cm^2. Although these cells were exposed to shear stress that impaired and delayed cell growth, which was not present in my study. Results from another research [49] found that a dual coating of gelatine (0.2%) and human fibronectin (2 µg/ml) extracellular matrix provided optimal cell attachment. In particular, this study concluded that by culturing HUVEC in defined media might help to retain their cell morphology and thus delay senescence. However, in my study, even by growing HUVEC in a defined media cell loss was encountered when the cell line was approaching senescence. In future studies, it might be beneficial to keep the cell seeding density high, while seeding the cells on a substrate that resembles the in vivo tissues as well as treating HUVEC with H_2O_2 to further delay senescence [50] and to enhance survival and proliferation.

Studies on Fixation

Initially cells were fixed with 4% PFA for 15 minutes at room temperature, yielding very poor results in terms of both cells density and cell morphology. Results from studies carried on paraformaldehyde fixation on plant cells pointed that long exposure to the compound might lead to dissociation of protein-protein or protein-nucleic acid interactions [51]. On the other hand, another research carried out on several cell lines concluded that cell morphology showed no alteration after being fixed with 4% PFA compared to their live counterparts [52]. However, it was concluded that that shrinkage or swelling after PFA exposure was cell specific [53].

As suggested by a fixation protocol from Abcam® [54] the PFA incubation time was lowered to 10 minutes. However, ten minutes was found to be excessive in my study for cells kept showing clear signs of membrane disruption. Incubation temperature increased to 37 °C from room temperature top try to achieve better fixation results as shown in a research carried over mKSA tumor cells found according to which the optimal fixation temperature was 37 °C when cells were exposed to 1% PFA [55]. However, after analysing cells with CLSM, membrane disruption was noted as well as the nanoemulsion signal being spread evenly inside the cells rather than clustered. Results were similar when decreasing the temperature to 0 °C. The integrity of nanoemulsions was found to be affected by the concentration of PFA as well as the incubation time since nanoemulsion consist of biological lipids [56]. Results from the research carried out from DiDonato et al. [56] on the fixation protocols showed that PFA was better than cold methanol for the latter caused lipid extraction from the cells and altered the appearance of lipid droplets visualized by microscopy. These results were particularly useful because they were in line with my observations. Eventually, evidences obtained through empirical testing suggested that cell morphology as well as nanoemulsion integrity were found optimal when fixing HUVEC with 3% PFA for 5 minutes at room temperature.

Studies on colocalization

The second aim of this research was to find evidence of signal colocalization between $\alpha_v\beta_3$ integrin and RGD conjugated nanoemulsions.

In a study carried out by Ruoslahti et al. [22], it was concluded that although the RGD sequence could be recognized by most of the integrin, the $\alpha_v\beta_3$ integrin was the most likely receptor to be involved in RGD pattern recognition and therefore binding. This led to the assumption that at any given time when integrin was present on the cell surface and not recycled [40, 57], and the RGD nanoemulsion were present, we should have observed colocalization. Particularly, we assumed that the degree of colocalization would be higher in HUVEC fixed immediately after nanoemulsion incubation than those re-incubated with medium. However, this appeared not to be the case.

By analysing the images from the different incubation times in figure 10, it was clear that there was almost no visible sign of colocalization. Although, this was not a strong evidence for the yellow signal was only detected is some sporadic regions of the cells in both the time points. Moreover, results from the analysis of cells with the Manders Colocalization Coefficients (table 4), showed no strong indication of signal co-occurrence. Although higher, the colocalization coefficients from the cells fixed immediately after 10 minutes of RGD nanoemulsion exposure were similar to those measured after 30 minutes of additional incubation time in medium. In particular, the Manders Colocalization Coefficients, tM2, reached their maximum peaks at 0.401 on the HUVEC fixed right away and 0.364 at after 30 minutes of incubation time. By observing these peaks, it was possible to obtain some evidences of colocalization. However, as table 5 reported, this was not a common trend. Moreover, this result was in line with the observation previously made on CLSM images of both time points.

During the study on signal colocalization, warnings were often encountered from the Coloc2 plug-in, in particular warnings such as "Y- interception being far from 0" and "high 0 – to – 0 values" were common in this study. According to literature, the tM1 and tM2 measure fluorescent signal colocalization [44]. While being independent from the signal intensities these coefficients are in fact affected by the background noise, and contributions from the PSF [58, 59]. The warning signs persisted after further background removal and further analysis of the images with other plug-ins such as Colocalization Threshold and Colocalization Test, deemed obsolete by Fiji, [60, 61] the same values of Manders colocalization coefficients were obtained. This was an important result because by backing up the original coefficients values obtained with Coloc2 we could rule out the hypothesis that images were biased therefore sustaining the claim that the signal colocalization was not wide spread through HUVEC at those time points.

This might be due to a fault in the methodology, poor staining and/or signal intensity. Additional studies on integrin-RGD-NE signal colocalization are required to unravel the precise reasons why colocalization was not observed. In the future, it might be beneficial to analyse live cells as well as fixed cells, taking images during multiple time points. It may be speculated that $\alpha_v\beta_3$ integrin could detach from the RGD-NE somewhere between 0 and 30 minutes and therefore the result obtained would justify the lack of signal colocalization without necessarily mean that colocalization is absent. This may also lead to the assumption that the binding period between $\alpha_v\beta_3$ integrin and RGD-NE is very short. Alas, data from research is too little to conclude anything on the matter.

Studies on nanoemulsion internalization patterns

The final aim of this study was to investigate nanoemulsion distribution patterns inside HUVEC over time as well as the difference in distribution between cells exposed to RGD conjugated nanoemulsions and RAD conjugated nanoemulsions.

As stated before, it has been well documented that the RGD motif binds to the β_3 subunit of the $\alpha_v\beta_3$ integrin [22, 62], and that the β_3 subunit of integrin and RGD forms clusters that would eventually be internalized via clathrin mediated endocytosis [16]. In my research, it was assumed that given the affinity for $\alpha_v\beta_3$ integrin, the RGD-NE would be internalized and carried to the perinuclear area. A research from Oba et al. [20] concluded that cyclic RGD molecules (c(RGDfK)), aided in the transport of poliplex micelles in the perinuclear region. Results from the 3D investigation of my study revealed that RGD conjugated nanoemulsions were carried inside the cell over time (figure 11, 13 and 15). These finding were in line with observation of Oba et al, [20, 21]. On the other hand, the RAD conjugated nanoemulsion was expected to be poorly internalized because of their lack of affinity for $\alpha_v\beta_3$ integrin [19]. However, by analysing the 3D renderings (figure 12, 14 and 16) it appeared not to be the case. The signal from these nanoemulsions appeared to be spread out the cells evenly. This might be due to the lack of internalization selectivity seen for the RGD motif as well as being internalized via macropinocytosis [17].

Results from the study involving the ROI analyses (Table 6 and 7) pointed that the differences between RGD and RAD conjugated nanoemulsion was not determined by signal intensity (voxels mean), rather signal distribution inside the cells over time. Oba et al, concluded in his research by conjugating ligands with the RGD motif, did not increase uptake, rather regulated intracellular trafficking [20]. This could explain why the voxel mean in cells incubated with RAD nanoemulsions was still significant (table 6). However, when analysing the

nanoemulsions distribution in function of time the RGD-NE appeared to move in the perinuclear area of the cells whereas the RAD-NE was spread evenly in cells and time appeared not to influence the nanoemulsion distribution. To remove signal intensity from the equation, results from table 6 were averaged in table 7 and the ratio between inner voxel mean versus the outer voxel mean was plotted in figure 18. By observing the latter, the differences in intracellular trafficking were striking, after 30 minutes of additional incubation the concentration of RGD conjugated nanoemulsion in the perinuclear region of the cells increased of almost two fold, whereas, the concentrations of the RAD conjugated nanoemulsion only slightly increased. Again, this finding confirms the previous research on RGD-NE internalization patterns [16, 20, 21, 62].

7 Conclusion

Through the experiment carried out in this this thesis optimal protocols for cell seeding, fixation and staining have been investigated. Cell plating efficiency ad well as density and morphology has been found to be optimal when cells were seeded in a concentration of 20.000 cells per µ-well in 300 µl of defined medium. Cells density and morphology was found to be satisfactory when cells were fixed for 5 minutes at room temperature with 300 µl of 3% Paraformaldehyde solution in PBS. Future studies to improve these protocols further might include seeding cells on a substrate resembling the in vivo condition investigated and treating HUVEC with H_2O_2 to delay senescence.

Colocalization studies between $\alpha_v\beta_3$ integrin and RGD conjugated nanoemulsions did not produced expected results, but multiple evidences from the literature suggests that colocalization does indeed takes place due to the numerous reports of RGD affinity to the $\alpha_v\beta_3$ integrin. Multiple reasons were speculated on why we did not observe this phenomenon. Remarkably, colocalization between the $\alpha_v\beta_3$ integrin and the RGD-NE might have happened in a short timeframe before integrin detached from RGD or else the "correct" time point during which colocalization is supposed to happen was not investigated. Moreover, the methods and/or the signal intensity from the integrin and or RGD-NE might not have been optimal therefore providing a false negative and giving biased results. For future studies, it is necessary to investigate this phenomenon by analysing multiple periods or even better by making an overtime imaging analysis while cells are live and incubating in the CLSM.

Eventually, 3D and ROI analyses of nanoemulsion internalization HUVEC over time confirmed previous hypothesis on internalization patterns and internal nanoemulsion distribution as well as difference of cellular uptake of RGD-NE and RAD-NE. CellMask™ and RAD-NE signal resolution could be improved in future studies.

1. 8 References

1. NIH, N.C.I. *What Is Cancer?* [cited 2016 1 May]; Available from: http://www.cancer.gov/about-cancer/understanding/what-is-cancer.
2. NIH, n.C.I. *A to Z List of Cancer Drugs*. [cited 2016 1 May]; Available from: http://www.cancer.gov/about-cancer/treatment/drugs.
3. WHO, W.H.O. *World Cancer Report 2014*. 2014 [cited 2016 1 May]; Available from: http://www.who.int/mediacentre/factsheets/fs297/en/.
4. Cai, W. and X. Chen, *Nanoplatforms for targeted molecular imaging in living subjects.* Small, 2007. **3**(11): p. 1840-54.
5. Wagner, V., et al., *The emerging nanomedicine landscape.* Nat Biotech, 2006. **24**(10): p. 1211-1217.
6. Cuenca, A.G., et al., *Emerging implications of nanotechnology on cancer diagnostics and therapeutics.* Cancer, 2006. **107**(3): p. 459-66.
7. Liu, Z., F. Wang, and X. Chen, *Integrin alpha(v)beta(3)-Targeted Cancer Therapy.* Drug Dev Res, 2008. **69**(6): p. 329-339.
8. Hsu, A.R., et al., *Integrin alpha v beta 3 antagonists for anti-angiogenic cancer treatment.* Recent Pat Anticancer Drug Discov, 2007. **2**(2): p. 143-58.
9. Kumar, C.C., *Integrin alpha v beta 3 as a therapeutic target for blocking tumor-induced angiogenesis.* Curr Drug Targets, 2003. **4**(2): p. 123-31.
10. Nakamura, H., F. Jun, and H. Maeda, *Development of next-generation macromolecular drugs based on the EPR effect: challenges and pitfalls.* Expert Opin Drug Deliv, 2015. **12**(1): p. 53-64.
11. Peer, D., et al., *Nanocarriers as an emerging platform for cancer therapy.* Nat Nano, 2007. **2**(12): p. 751-760.
12. Prabhakar, U., et al., *Challenges and key considerations of the enhanced permeability and retention effect for nanomedicine drug delivery in oncology.* Cancer Res, 2013. **73**(8): p. 2412-7.
13. Teklemariam, T., et al., *Functional analysis of a recombinant PIII-SVMP, GST-acocostatin; an apoptotic inducer of HUVEC and HeLa, but not SK-Mel-28 cells.* Toxicon, 2011. **57**(5): p. 646-56.
14. Ciechanowska, A., et al., *Human endothelial cells hollow fiber membrane bioreactor as a model of the blood vessel for in vitro studies.* J Artif Organs, 2016.
15. Brooks, P.C., R.A. Clark, and D.A. Cheresh, *Requirement of vascular integrin alpha v beta 3 for angiogenesis.* Science, 1994. **264**(5158): p. 569-71.
16. Yu, C.H., et al., *Integrin-beta3 clusters recruit clathrin-mediated endocytic machinery in the absence of traction force.* Nat Commun, 2015. **6**: p. 8672.
17. Kou, L., et al., *The endocytosis and intracellular fate of nanomedicines: Implication for rational design.* Asian Journal of Pharmaceutical Sciences, 2013. **8**(1): p. 1-10.
18. Schroeder, A., et al., *Treating metastatic cancer with nanotechnology.* Nat Rev Cancer, 2012. **12**(1): p. 39-50.
19. Cressman, S., et al., *Binding and Uptake of RGD-Containing Ligands to Cellular α v β 3 Integrins.* International Journal of Peptide Research and Therapeutics, 2009. **15**(1): p. 49-59.
20. Oba, M., et al., *Polyplex micelles with cyclic RGD peptide ligands and disulfide cross-links directing to the enhanced transfection via controlled intracellular trafficking.* Mol Pharm, 2008. **5**(6): p. 1080-92.

21. Oba, M., et al., *Cyclic RGD peptide-conjugated polyplex micelles as a targetable gene delivery system directed to cells possessing alphavbeta3 and alphavbeta5 integrins.* Bioconjug Chem, 2007. **18**(5): p. 1415-23.
22. Ruoslahti, E., *RGD and other recognition sequences for integrins.* Annu Rev Cell Dev Biol, 1996. **12**: p. 697-715.
23. Danhier, F., A.L. Breton, and V. Préat, *RGD-Based Strategies To Target Alpha(v) Beta(3) Integrin in Cancer Therapy and Diagnosis.* Molecular Pharmaceutics, 2012. **9**(11): p. 2961-2973.
24. Knudson, A.G., Jr., *Mutation and cancer: statistical study of retinoblastoma.* Proc Natl Acad Sci U S A, 1971. **68**(4): p. 820-3.
25. Muthukkaruppan, V.R., L. Kubai, and R. Auerbach, *Tumor-induced neovascularization in the mouse eye.* J Natl Cancer Inst, 1982. **69**(3): p. 699-708.
26. Flintoft, L., *Recruitment drive.* Nat Rev Cancer, 2004. **4**(8): p. 575-575.
27. Thompson, R.H., et al., *Metastatic renal cell carcinoma risk according to tumor size.* J Urol, 2009. **182**(1): p. 41-5.
28. Burns, M.P. and N. DePaola, *Flow-conditioned HUVECs support clustered leukocyte adhesion by coexpressing ICAM-1 and E-selectin.* Am J Physiol Heart Circ Physiol, 2005. **288**(1): p. H194-204.
29. Kokura, S., et al., *Molecular mechanisms of neutrophil-endothelial cell adhesion induced by redox imbalance.* Circ Res, 1999. **84**(5): p. 516-24.
30. Zhang, W., et al., *Communication between malignant glioma cells and vascular endothelial cells through gap junctions.* J Neurosurg, 2003. **98**(4): p. 846-53.
31. Hood, J.D. and D.A. Cheresh, *Role of integrins in cell invasion and migration.* Nat Rev Cancer, 2002. **2**(2): p. 91-100.
32. Grodzinski, P., M. Silver, and L.K. Molnar, *Nanotechnology for cancer diagnostics: promises and challenges.* Expert Rev Mol Diagn, 2006. **6**(3): p. 307-18.
33. Ryan, S.M., et al., *Advances in PEGylation of important biotech molecules: delivery aspects.* Expert Opin Drug Deliv, 2008. **5**(4): p. 371-83.
34. Howard, M.D., et al., *PEGylation of Nanocarrier Drug Delivery Systems: State of the Art.* Journal of Biomedical Nanotechnology, 2008. **4**(2): p. 133-148.
35. Jain, R.K., *Transport of molecules across tumor vasculature.* Cancer Metastasis Rev, 1987. **6**(4): p. 559-93.
36. Claxton, N.S., T.J. Fellers, and M.W. Davidson, *Microscopy, Confocal*, in *Encyclopedia of Medical Devices and Instrumentation*. 2006, John Wiley & Sons, Inc.
37. Leica. *The Hybrid Detector Leica HyD*. [cited 2016 1 may]; Available from: http://www.leica-microsystems.com/products/confocal-microscopes/details/product/leica-hyd/.
38. Jarzyna, P.A., et al., *Iron oxide core oil-in-water emulsions as a multifunctional nanoparticle platform for tumor targeting and imaging.* Biomaterials, 2009. **30**(36): p. 6947-54.
39. ThermoFisher. *CellMask™ Deep Red Plasma membrane Stain*. [cited 2016 1 May]; Available from: https://www.thermofisher.com/order/catalog/product/C10046.
40. Roberts, M., et al., *PDGF-regulated rab4-dependent recycling of alphavbeta3 integrin from early endosomes is necessary for cell adhesion and spreading.* Curr Biol, 2001. **11**(18): p. 1392-402.
41. Schindelin, J., et al., *Fiji: an open-source platform for biological-image analysis.* Nat Methods, 2012. **9**(7): p. 676-82.
42. Daniel J. White, T.K., Johannes Schindelin *Coloc 2 - Standardized, modular, Pixel Intensity Correlation over Space Based Colocalization analysis. (ImageJ - Fiji - ImgLib)*. 26 Feb 2015 Available from: http://imagej.net/Coloc_2.

43. Costes, S.V., et al., *Automatic and quantitative measurement of protein-protein colocalization in live cells.* Biophys J, 2004. **86**(6): p. 3993-4003.
44. Manders, E.M.M., F.J. Verbeek, and J.A. Aten, *Measurement of co-localization of objects in dual-colour confocal images.* Journal of Microscopy, 1993. **169**(3): p. 375-382.
45. Huang, C.C., et al., *Enhancement of cell adhesion, retention, and survival of HUVEC/cbMSC aggregates that are transplanted in ischemic tissues by concurrent delivery of an antioxidant for therapeutic angiogenesis.* Biomaterials, 2016. **74**: p. 53-63.
46. Scheller, K. and B. Frerich, *Ca(2+)-deposition in cell matrix correlates significantly with osteocalcin-expression in osteogenic differentiated ATSC: Even in a coculture system with HUVEC.* J Oral Maxillofac Pathol, 2013. **17**(3): p. 340-5.
47. Kakinoki, S., et al., *A large mobility of hydrophilic molecules at the outmost layer controls the protein adsorption and adhering behavior with the actin fiber orientation of human umbilical vein endothelial cells (HUVEC).* J Biomater Sci Polym Ed, 2013. **24**(11): p. 1320-32.
48. Heng, B.C., et al., *Effect of cell-seeding density on the proliferation and gene expression profile of human umbilical vein endothelial cells within ex vivo culture.* Cytotherapy, 2011. **13**(5): p. 606-17.
49. Bala, K., K. Ambwani, and N.K. Gohil, *Effect of different mitogens and serum concentration on HUVEC morphology and characteristics: implication on use of higher passage cells.* Tissue Cell, 2011. **43**(4): p. 216-22.
50. Ruan, Y., et al., *Retarding the senescence of human vascular endothelial cells induced by hydrogen peroxide: effects of 17beta-estradiol (E2) mediated mitochondria protection.* Biogerontology, 2014. **15**(4): p. 367-75.
51. Li, M.W., L. Zhou, and H.M. Lam, *Paraformaldehyde Fixation May Lead to Misinterpretation of the Subcellular Localization of Plant High Mobility Group Box Proteins.* PLoS One, 2015. **10**(8): p. e0135033.
52. Su, J.W., et al., *Investigation of influences of the paraformaldehyde fixation and paraffin embedding removal process on refractive indices and scattering properties of epithelial cells.* J Biomed Opt, 2014. **19**(7): p. 75007.
53. CRAWFORD, C.N.C. and R. BARER, *The Action of Formaldehyde on Living Cells as Studied by Phase-contrast Microscopy.* Journal of Cell Science, 1951. **s3-92**(20): p. 403-452.
54. abcam. *IHC fixation protocol*. [cited 2016 1 May]; Available from: http://www.abcam.com/protocols/ihc-fixation-protocol.
55. Oikawa, T., et al., *Temperature-dependent alteration in immunogenicity of tumor-associated transplantation antigen monitored via paraformaldehyde fixation.* Cancer Res, 1979. **39**(9): p. 3519-23.
56. DiDonato, D. and D.L. Brasaemle, *Fixation methods for the study of lipid droplets by immunofluorescence microscopy.* J Histochem Cytochem, 2003. **51**(6): p. 773-80.
57. Hak, S., et al., *Periodicity in tumor vasculature targeting kinetics of ligand-functionalized nanoparticles studied by dynamic contrast enhanced magnetic resonance imaging and intravital microscopy.* Angiogenesis, 2014. **17**(1): p. 93-107.
58. Abraham, T., S.E. Allan, and M.K. Levings, *Deconvolution and chromatic aberration corrections in quantifying colocalization of a transcription factor in three-dimensional cellular space.* Micron, 2010. **41**(6): p. 633-40.
59. Dunn, K.W., M.M. Kamocka, and J.H. McDonald, *A practical guide to evaluating colocalization in biological microscopy.* Am J Physiol Cell Physiol, 2011. **300**(4): p. C723-42.

60. Collins, T. *Colocalization Threshold (ImageJ - Fiji)*. june 2009 [cited 2016 1 May]; Available from: http://imagej.net/Colocalization_Threshold.
61. Collins, T. *Colocalization Test (ImageJ - Fiji)*. june 2009 [cited 2016 1 May]; Available from: http://imagej.net/Colocalization_Test.
62. Smith, J.W. and D.A. Cheresh, *The Arg-Gly-Asp binding domain of the vitronectin receptor. Photoaffinity cross-linking implicates amino acid residues 61-203 of the beta subunit.* J Biol Chem, 1988. **263**(35): p. 18726-31.